

# Changes in U.S. temperature extremes under increased CO<sub>2</sub> in millennial-scale climate simulations

Whitney K. Huang<sup>1</sup>, Michael L. Stein<sup>2</sup>, David J. McInerney<sup>3</sup>, Shanshan Sun<sup>4</sup>, and Elisabeth J. Moyer<sup>4</sup>

<sup>1</sup>Department of Statistics, Purdue University

<sup>2</sup>Department of Statistics, University of Chicago

<sup>3</sup>School of Civil, Environmental and Mining Engineering, University of Adelaide

<sup>4</sup>Department of the Geophysical Sciences, University of Chicago

## Abstract

Changes in extreme weather may produce some of the largest societal impacts from anthropogenic climate change: present-day weather damages are dominated by rare events that happen only every several decades or more. However, it is intrinsically difficult to estimate changes in those rare events from the short observational record. We therefore look for insight to climate models where we can generate long simulations. In this work we use millennial runs from the Community Climate System Model version 3 (CCSM3) in equilibrated pre-industrial and possible future (700 and 1400 ppm CO<sub>2</sub>) conditions to examine both how extremes change and how well these changes can be estimated as a function of run length. We estimate changes to distributions of future seasonal temperature extremes (wintertime minima and summertime maxima) in the contiguous United States by fitting generalized extreme value (GEV) distributions using the block maxima approach. Using 1000-year pre-industrial and future time series, we show that the magnitude of summer warm extremes largely shifts in accordance with mean shifts in summertime temperatures, and their distribution does not otherwise change significantly. In contrast, winter cold extremes warm more than mean shifts in wintertime temperatures, with changes in spread and skewness at inland locations that lead to substantial changes in tail behavior. We then examine uncertainties that result from using shorter model runs. In principle, GEV modeling allows us to predict infrequent events using time series shorter than the recurrence frequency of those events. To investigate how well this approach works in practice, we estimate 20-, 50-, and 100-year extreme events using segments of varying length. We find that even with GEV modeling, time series that are of comparable length or shorter than the return period of interest can lead to very poor estimates. These results suggest caution when attempting to use short observational time series/model runs to infer infrequent extremes.

## 1 Introduction

As the Earth's mean climate changes under increased concentrations of human-emitted greenhouse gases, the intensity and frequency of extreme weather conditions may change as well (Easterling et al., 2000, chapter 11: IPCC, 2014 and reference therein). Extreme events, while rare by definition, can have large impacts on both human society and environmental systems: present-day weather damages are dominated by rare events that happen only every several decades or more (see (NOAA, 2015, <https://www.ncdc.noaa.gov/billions/>)), and society's vulnerability to extreme events appears to be growing (Kunkel et al., 1999). In the United States, the frequency of climate and weather events with damages greater than \$1 billion appears to be increasing at around 5% per year (Smith and Katz, 2013). It remains unclear to what extent long-term climate trends contribute to that rise, but these factors have led to extensive efforts to understand the relationship between long-term climate change

driven by greenhouse gas forcing and potential changes in climate extremes. Studies have sought to identify changes in climate extremes both in observations over the past century (Easterling et al., 2000; Tebaldi et al., 2006; Shaby and Reich, 2012; Naveau et al., 2014; Westra et al., 2013; Lee et al., 2014) and in general circulation model (GCM) simulations of future climates (Kharin and Zwiers, 2000; Kharin et al., 2007, 2013; Sterl et al., 2008; Frías et al., 2012).

Analysis of changes in extremes is complicated by the fact that there is no unique definition of "extremes". One common definition is as exceedance of certain defined thresholds, with threshold values often defined based on past climate distributions (e.g. Frich et al., 2002; Alexander et al., 2006; Tebaldi et al., 2006). Analyses then evaluate changes in the frequencies at which these thresholds are surpassed. Alexander et al. (2006), for example, used percentile-based thresholds for various climate metrics from three decades of global gridded observations (1961-1990) and then considered changes in a subsequent period (1991-2003). They found a significant increase in the occurrence of annual warm nights (defined as the 90% quantiles of daily minimum temperature under the past climate) and a significant decrease in the occurrence of cold nights (defined as the 10% quantiles of daily minimum temperature under the past climate).

However, many threshold exceedance studies do not explicitly compare extreme changes to those expected from mean shifts. Furthermore, nearly all studies evaluate only a single aspect of a potentially shifting marginal distribution of climate. That is, they do not characterize changes in the shape of a distribution by making use of information on the magnitude of exceedances above (below) the defined threshold. Some methods do assess the distribution of threshold exceedances, e.g. approaches based on generalized Pareto distribution (GPD) (Pickands III, 1975; Smith, 1989; Davison and Smith, 1990), but their utility depends on choosing appropriate thresholds for present and future climate. That choice is difficult a priori before results are known, perhaps contributing to the relatively limited application of these approaches in climate science.

An alternate and potentially more useful definition of "extremes" is based not on the marginal distribution of a climate variable but on the distribution of extreme occurrences in its far tail. In the extreme value theory (EVT) approach (Fisher and Tippett, 1928; Gumbel, 1958; Coles et al., 2001; Katz et al., 2002), one first defines a "block extreme" as the maximum (minimum) of some climate variable over a given block of time; in climate studies, blocks of one year are common (e.g. Zwiers and Kharin, 1998). The magnitudes of these extremes over a long time period (i.e. block size) are then approximately described by the generalized extreme value (GEV) distribution. The approximation is valid under a range of assumptions (Gnedenko, 1943, Leadbetter et al., 1983, and see chapter 1 of de Haan and Ferreira, 2006 for details); in these conditions, the tail behavior of most distributions can be described by a functional form involving only three parameters (the location, scale, and shape parameters of the GEV distribution). For example, the widely used measure of extreme events,  $r$ -year return level, can be derived from the corresponding GEV. See Section 3 for further review: Figure 1 illustrates how changes in block extremes can differ from changes in the underlying overall distribution, using seasonal temperature minima from millennial-scale climate model runs, and Figure 3 in Section 3.2 illustrates the effect on the return levels of changing each individual GEV parameter.

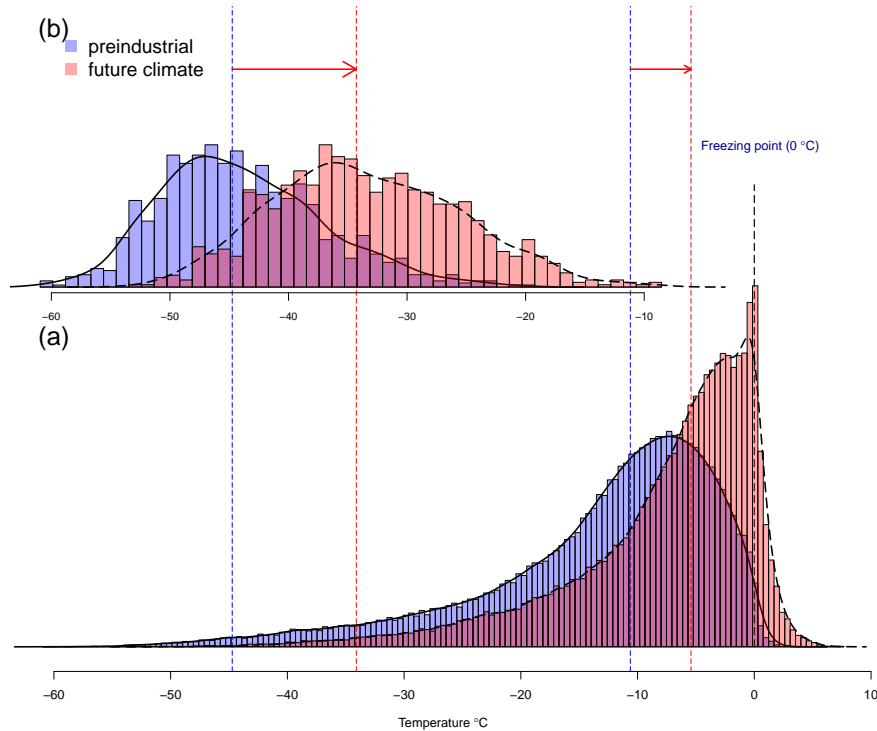


Figure 1: Illustration of how the changes in the distribution of extremes can differ from the changes in an overall distribution. Data shown are wintertime (December-January-February (DJF)) temperatures in a location in Idaho from two of the 1000-year CCSM3 model runs used in this study, with  $\text{CO}_2$  concentrations of 289 (pre-industrial, blue) and 700 ppm (future climate, red). **(a)**: Distributions of winter daily minimum temperature ( $T_{\min}$ ). **(b)**: Distributions of seasonal minimum winter  $T_{\min}$ . Note several features: 1) in both climate states, the distributions of seasonal minima are skewed to the right whereas their marginal distributions are skewed to the left; 2) in the future warmer climate state, variation in the marginal distribution decreases but variation in the seasonal minima increases; 3) the median of the distribution of seasonal minima increases more than the median of the marginal distribution. The distortion in the distribution of daily temperature at  $0^\circ\text{C}$  occurs because latent heat provides a barrier to freezing or thawing; this effect is more pronounced in models than in real data. The version of summertime (JJA) at this location is shown in Appendix A.1 Fig. A.1.

The EVT approach has advantages for study of climate extremes, because it allows characterizing changes in events that are more rare than the “moderate extremes” analyzed in threshold exceedance studies. Alexander et al. (2006) used a threshold equivalent to the 90% quantile of 5 day sliding window over 1961~1990, i.e. they examine temperature events whose present mean recurrence interval is approximately two months. EVT theory allows examining rare events of much longer recurrence intervals. In principle, it allows even extrapolation into the far tail of a distribution, i.e. predicting beyond the observed range given a finite time series, with a measure of statistical uncertainty. The EVT approach has been widely applied in hydrology, for example, to estimate 100-year floods using several decades of data (Katz et al., 2002).

In the past two decades, the EVT approach has been applied to climate variables, generally temperature and precipitation, by numerous authors (including Zwiers and Kharin, 1998; Kharin and Zwiers, 2005; Kharin et al., 2007; Sterl et al., 2008; Frías et al., 2012; Kharin et al., 2013; Craigmile et al., 2013). Studies have evaluated GEV distributions both in observational data and in output from general circulation model (GCM) and regional climate model (RCM) simulations. Kharin et al.

(2007, 2013) evaluated GCM ensembles from the Coupled Model Intercomparison Project Phase 3 and Phase 5 (CMIP3 and CMIP5) under several projected emission scenarios. In both studies they found asymmetry in extreme changes, with high temperature extremes in most regions following changes in the mean summer temperature whereas low temperature extremes warming substantially more than mean winter temperatures. Asymmetry in extreme changes occurs especially in regions where snow and sea-ice retreat with global warming.

Prior GEV studies are limited to some extent by two factors: the length of analyzed time series, and their non-stationarity. For observational studies, existing data records are relatively short (only several decades). Model ensembles are longer, but the model runs used in these studies typically extend only around 100 years from the present, and ensembles often include only one or a few model realizations. Time series length matters strongly for detecting changes in extremes: a too-short record can lead to large uncertainty in estimated return levels for periods long relative to the time series (see Section 6). Secondly, at present and for the foreseeable future, the Earth’s climate is not in equilibrium but is evolving (transient), so the GEV model must be extended to account for non-stationarity in climate extremes. The means of extension are not trivial. The most commonly used nonstationary GEV model (e.g. Kharin and Zwiers, 2005) assumes that location and scale parameters change linearly in time and the shape parameter is time-invariant; this model may not be flexible enough for representing climate data.

In this study we overcome these limitations by using three long (millennial) climate model runs in which climate is fully equilibrated. While numerical simulations of future climates provide only suggestions for possible changes in climate variables, not direct evidence of changes, they are necessary complements to observational studies. In this work we use temperature output from the widely used Community Climate System 3 (CCSM3) model (Collins et al., 2006; Yeager et al., 2006) at three different CO<sub>2</sub> levels. In all runs the climate has fully responded to forcing changes, so that any time series of block extremes forms a stationary sequence. The use of long stationary runs should allow a more accurate determination of any changes in GEV distributions than the shorter runs of the CMIP archives. Furthermore, the three different climate states allow us to evaluate the linearity of changes in extremes with mean temperature change. The long model runs also allow us to assess the appropriateness of the choice of annual or seasonal blocks, which are conventional in part simply because longer blocks would be infeasible for the shorter (century-scale) climate model runs typically used. In our case we can test, based on the max-stable property of GEV (see Section 5 for details), whether seasonal blocks are indeed appropriate. Finally, the long runs allow us to evaluate sampling errors when estimating extreme return levels in shorter model runs.

The paper is structured as follows: in Section 2, we describe the model output used in this work; in Section 3, we provide the background of the univariate extreme value theory we employ; in Section 4, we describe the changes in extreme value distributions and corresponding return levels, and compare them with changes in climate means. In Section 5 we assess the sensitivity of those results to block length, and in Section 6 we assess the sensitivity of those results to time series length. We conclude with a discussion of the implications of these results.

## 2 GCM Output

The GCM output used is part of an ensemble of climate simulations completed by the Center for Robust Decision Making on Climate and Energy Policy (RDCEP) (e.g. Castruccio et al., 2014; Leeds et al., 2015), using the Community Climate System Model version 3 (CCSM3), a fully-coupled model with full representation of the atmosphere (CAM3), land (CLM3), sea ice (CSIM5) and ocean (POP 1.4.3) components. The model was run at the relatively coarse T31 spatial resolution ( $3.75^\circ \times 3.75^\circ$  grid), which made possible the lengthy runs used here. We use here the last 1000 years of output from each of three multimillennial runs with different atmospheric CO<sub>2</sub> concentrations: 289 ppm (pre-industrial), 700 ppm (3.4 °C increase in global mean temperature (GMT)), and 1400 ppm (6.1 °C



increase in GMT). In each case, solar forcing, aerosol concentrations, and concentrations of greenhouse gases other than CO<sub>2</sub> are kept at their pre-industrial values. The final 1000 years of each model run are very nearly in equilibrium: net global radiative imbalances at the surface and at top-of-atmosphere (TOA) are smaller than 0.1 W m<sup>-2</sup>. The model’s temperature output therefore forms a stationary time series. For convenience we restrict our analysis to the contiguous United States and adjacent ocean regions (see Fig. 2).

In this work, we consider not annual but seasonal maxima and minima, following a standard practice in the literature (e.g. Smith, 1989). That is, for each year we take the maximum summertime (JJA) daily maximum temperature ( $T_{\max}$ ) and the minimum wintertime (DJF) minimum temperatures ( $T_{\min}$ ). For most inland locations, the distinction between annual and seasonal extremes is negligible:  $\approx 90\%$  of annual maxima or minima fall in their expected corresponding season (summer or winter) (see Fig. A.2 in Appendix A.2). As a result, the GEV distributions and changes in return levels are almost identical for both cases ( Appendix A.2 Fig. A.4). Ocean locations show a less distinct seasonal cycle, so that a lower percentage of extremes fall in the “appropriate” season (see e.g. Fig. S2b in Appendix A.2), but estimates of return level changes are unaffected by the choice of annual or seasonal extremes, presumably because changes in GEV distributions are dominated by simple shifts in the location parameter. However, in a few inland locations in the U.S. Midwest, the use of seasonal maxima is problematic: a significant fraction (as high as 46%) of annual maxima fall outside summer (Fig. S2d in Appendix A.2), and return level estimates from seasonal and annual extremes diverge (generally because of differences in shape parameter estimates).

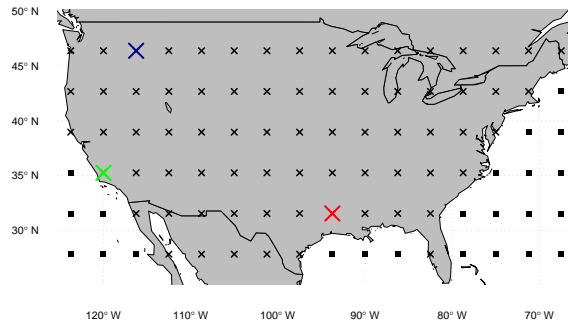


Figure 2: Locations of center of grid cells for model output used here (crosses for inland pixels and boxes for ocean pixels). Pixels marked with large crosses (Idaho, (dark blue), California, (green), and Texas, (red)) are used as examples throughout this study.

### 3 Statistical Background

The GEV distribution is widely applicable in the sciences because it arises, at least approximately, in many cases of natural data. The simplest situation where a GEV distribution can arise is in distributions of maxima taken from sequences of  $n$  independent and identically distributed (i.i.d.) random variables ( $Y_1, \dots, Y_n$ ), with “block length”  $n$  sufficiently large. The Extremal Types Theorem says that if the maxima  $M_n = \max(Y_1, \dots, Y_n)$ , after normalization (i.e.  $\frac{M_n - b_n}{a_n}$ ,  $a_n > 0$ ), converge in distribution as  $n \rightarrow \infty$  (see Appendix A.3), then they converge to a GEV distribution (Fisher and Tippett, 1928; Gnedenko, 1943).

In this work, when studying summer warm temperature extremes, the variables  $Y_1, \dots, Y_n$  are the daily maximum temperatures, and the block length  $n$  is 92 days, so that the  $M_n$  are annual summer temperature highs. Of course time series of daily temperatures are neither independent (they are

somewhat autocorrelated) nor identically distributed (their distributions may vary within a season). There is theoretical justification for the use of GEV distributions in our case: it has been shown that the independence assumption can be relaxed for weakly dependent stationary time series (Leadbetter et al., 1983; Hsing, 1991), and Einmahl et al. (2015) extended the theory to non-identically-distributed observations with conditions on the tail distributions (e.g. distributions share a common absolute maximum). In this work, we explicitly assess whether the inferred GEV distribution actually provides adequate description of the dataset in question. The CCSM3 temperature time series studied here do seem to meet this condition: quantile–quantile plots show that the GEV approximation appears to fit reasonably well for most pixels in our study area (see Fig. A.5 and Fig. A.6 in Appendix A.4). We therefore assume that annual summer maxima and winter minima of daily temperature in our model output can be approximated by GEV distributions. We will revisit the assessment of the GEV approximation in Section 5 when we test whether our block length  $n$  is sufficient.

### 3.1 GEV distributions

We give here a brief review of GEV theory. For further background, de Haan and Ferreira (2006) and Resnick (1987, 2007) provide systematic theoretical accounts and Coles et al. (2001) and Beirlant et al. (2004) describe statistical treatments. The GEV distribution function, described in terms of its three parameters  $\mu$ ,  $\sigma$ , and  $\xi$ , is

$$G_{\mu,\sigma,\xi}(y) = \begin{cases} \exp\left(-\left\{1 + \frac{\xi(y-\mu)}{\sigma}\right\}_+^{-\frac{1}{\xi}}\right) & \xi \neq 0 \\ \exp\left(-\exp\left\{\frac{-(y-\mu)}{\sigma}\right\}\right) & \xi = 0 \end{cases} \quad (1)$$

where the subscript  $+$  denotes the greater of a quantity and zero (i.e. for any variable  $u$ ,  $u_+ = \max(0, u)$ ). If the shape parameter  $\xi$  is zero, then the distribution is an *exponentially-tailed* Gumbel distribution, with the location parameter  $\mu$  describing the mode of the distribution and the scale parameter  $\sigma$  describing its spread. When non-zero, the shape parameter  $\xi$  determines the tail behavior of the density. Cases with  $\xi > 0$  correspond to the *heavy-tailed* Fréchet distribution and those with  $\xi < 0$  to the *bounded-tailed* reversed Weibull distribution, in which the distribution has an absolute maximum  $\mu - \sigma/\xi$ . Distributions of temperature extremes typically have  $\xi < 0$ : that is, temperatures do not exceed certain threshold values.

For studying winter temperature extremes, we must consider minima rather than maxima. Equation (1) can be used to study minima simply by considering that the maximum of  $-Y_1, \dots, -Y_n$ , where  $Y_i$  represents the winter daily minimum temperature on day  $i$ . However, if one lets  $(\mu, \sigma, \xi)$  be the parameters for the corresponding GEV distribution of the maximum of the negative temperature, then increasing  $\mu$  would correspond to decreasing temperature, which we find potentially confusing. We therefore adopt the convention that when considering winter temperature minima, we will write for the corresponding GEV distribution

$$G_{\mu,\sigma,\xi}(y) = \begin{cases} \exp\left(-\left\{1 + \frac{\xi(\mu-y)}{\sigma}\right\}_+^{-\frac{1}{\xi}}\right) & \xi \neq 0 \\ \exp\left(-\exp\left\{\frac{-(\mu-y)}{\sigma}\right\}\right) & \xi = 0 \end{cases} \quad (2)$$

With this definition, a larger  $\mu$  corresponds to warmer temperature minima. In the remainder of this work, we assume that for summer maxima, the relevant GEV distribution is (1), and for winter minima, the relevant distribution is (2).

### 3.2 Relationship between GEV Distributions and Return Levels

In the analysis that follows, we also describe extremes by their return levels, a widely used measure of extreme events. For warm temperature extremes, the  $r$ -year return level is the (block maximum) temperature exceeded on average once per  $r$  years. Note that the concept of return levels implicitly assumes equilibrated, stationary conditions. Return levels in a dataset whose extremes follow a GEV distribution can be written in terms of the GEV parameters. Letting  $p = 1/r$ , the  $r$ -year return level  $y_p$  is the  $100 \times (1 - p)$ th quantile of the underlying GEV distribution, which can be determined by solving the equation  $G(y_p) = 1 - p$  (for  $0 < p < 1$ ) to obtain:

$$y_p = \begin{cases} \mu - \frac{\sigma}{\xi} \left\{ 1 - (-\log(1 - p))^{-\xi} \right\} & \xi \neq 0 \\ \mu - \sigma \log(-\log(1 - p)) & \xi = 0 \end{cases} \quad (3)$$

where the “log” denotes the natural logarithm. A similar result holds for temperature minima.<sup>1</sup>

In the warmer climate conditions that result from higher atmospheric CO<sub>2</sub>, the GEV distributions of temperature extremes may change, altering return levels. Changes in the different GEV parameters affect return levels in different ways. In Figure 3, we illustrate the consequences on both distributions and return levels of changing each GEV parameter. Changing the location parameter  $\mu$  simply shifts the distribution of extremes by the change  $\Delta\mu$  and changes levels uniformly at all return periods by the same amount (Fig. 3 top row). Changing the scale parameter  $\sigma$  broadens or narrows the distribution of extremes. That effect exacerbates extremes at long return periods and mitigates them at short return periods (Fig. 3 middle row). There is no effect at  $(1 - p) = e^{-1}$  or  $r = e/(e - 1) \approx 1.6$  years. The changes in return levels are approximately linear with return period around this point, and faster than linearly at both tails.

Changing the shape parameter  $\xi$  alters the “heaviness” of the tails, but does so asymmetrically, with the greatest extremes most strongly affected (the high temperature tail for maxima, and the low temperature tail for minima). The resultant changes in return levels are then highly nonlinear with return period. Changing  $\xi$  has negligible effect on return levels for periods less than 10 years, but strongly affects the “extreme extremes” at long return periods.

In practice, as GEV distributions shift under higher CO<sub>2</sub> concentrations, the effect of a shifted location parameter is easiest to distinguish. Changes in the scale and shape parameters affect the tails of the distribution of extremes, and the shape parameter eventually dominates the far tail.

---

<sup>1</sup>Note that equation 3 implicitly assumes block lengths of 1 year and must be changed for different block lengths: the definition of  $p$  becomes  $p = b/r$ , where  $b$  is the block length in years. The differences in  $r$ -year return levels defined by different block lengths are largest for the shortest return periods (largest  $p$ ) and become negligible for multi-decadal return periods ( $p$  becomes close to 0).

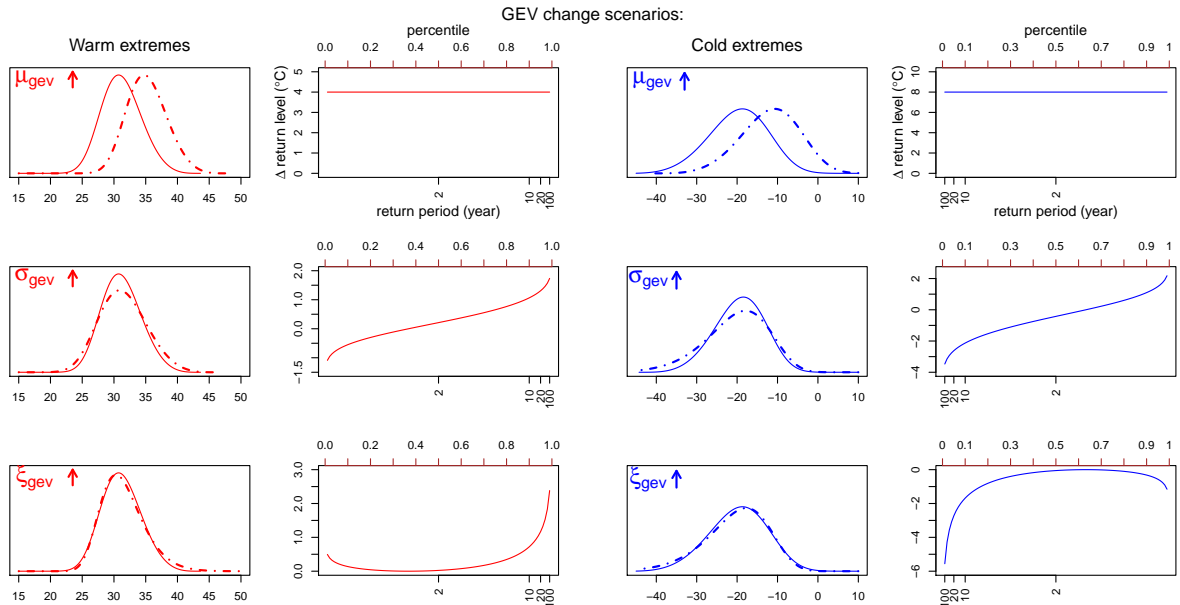


Figure 3: Illustration of the effect on return levels of changing individual GEV parameters. We show consequences for both summertime warm (red, left columns) and wintertime cold (blue, right columns) extremes. Columns 1 and 3 show GEV distributions for baseline (solid) and future (dashed) climates. Columns 2 and 4 show resulting changes in return levels for different return periods. (Note that 100-year periods are on the right for warm and left for cold extremes, to conform with percentiles.) The changes in location and shape parameters used here are chosen as representative of our model results, with larger effects in winter than summer, while changes in shape parameter are identical in both seasons. **Top row**: changing the location parameter shifts return levels uniformly across return periods. **Middle row**: increasing the scale parameter produces effects dependent on return period. Return levels become extreme at short periods but more extreme at long periods, where they increase linearly with period until roughly 20 years and become faster than linearly in the tail. **Bottom row**: increasing the shape parameter produces changes in return levels that are highly nonlinear with return period, with small changes at short return periods and then exponential increases in the tail.

## 4 Results

By fitting the seasonal temperature maxima and minima to a GEV distribution (see Appendix A.5 for fitting GEV parameters), we can identify changes in the distribution of extremes in possible future warmer climates, and evaluate how the characteristics of those changes produce changes in return levels of extreme events. We show results here for all three model runs (pre-industrial, 700 ppm, and 1400 ppm.) By using two different future climate states, we can also assess the linearity of changes in the extremes with changes in mean temperatures.

### 4.1 GEV parameters in preindustrial and future climates

We show in Figure 4 the estimated CCSM3 GEV parameters for summer and winter temperature extremes over the North American region. We show maps of GEV parameter values for the pre-industrial climate (left column), and maps of changes between pre-industrial and 700 ppm (middle column) and between 700 and 1400 ppm (right column). The fitted GEV parameters of the pre-industrial run show spatially coherent patterns, with both latitudinal gradients and land-ocean contrast that are consistent with expectations. As expected, the location parameters for summertime warm extremes are highest where summers are warmest, in the desert Southwest and the inland Northeast/Midwest. Similarly, for

wintertime cold extremes,  $\mu$ 's are lowest where winters are coldest: their pattern is a strong latitudinal gradient, but moderated along the coasts.

The scale parameter, which affects the spread of the distribution of extremes, is largest in the continental interior and very small over the ocean, as expected. The shape parameter, which affects the far tail of the distribution of extremes, is negative nearly everywhere, as is usually the case for a time series of surface temperatures.

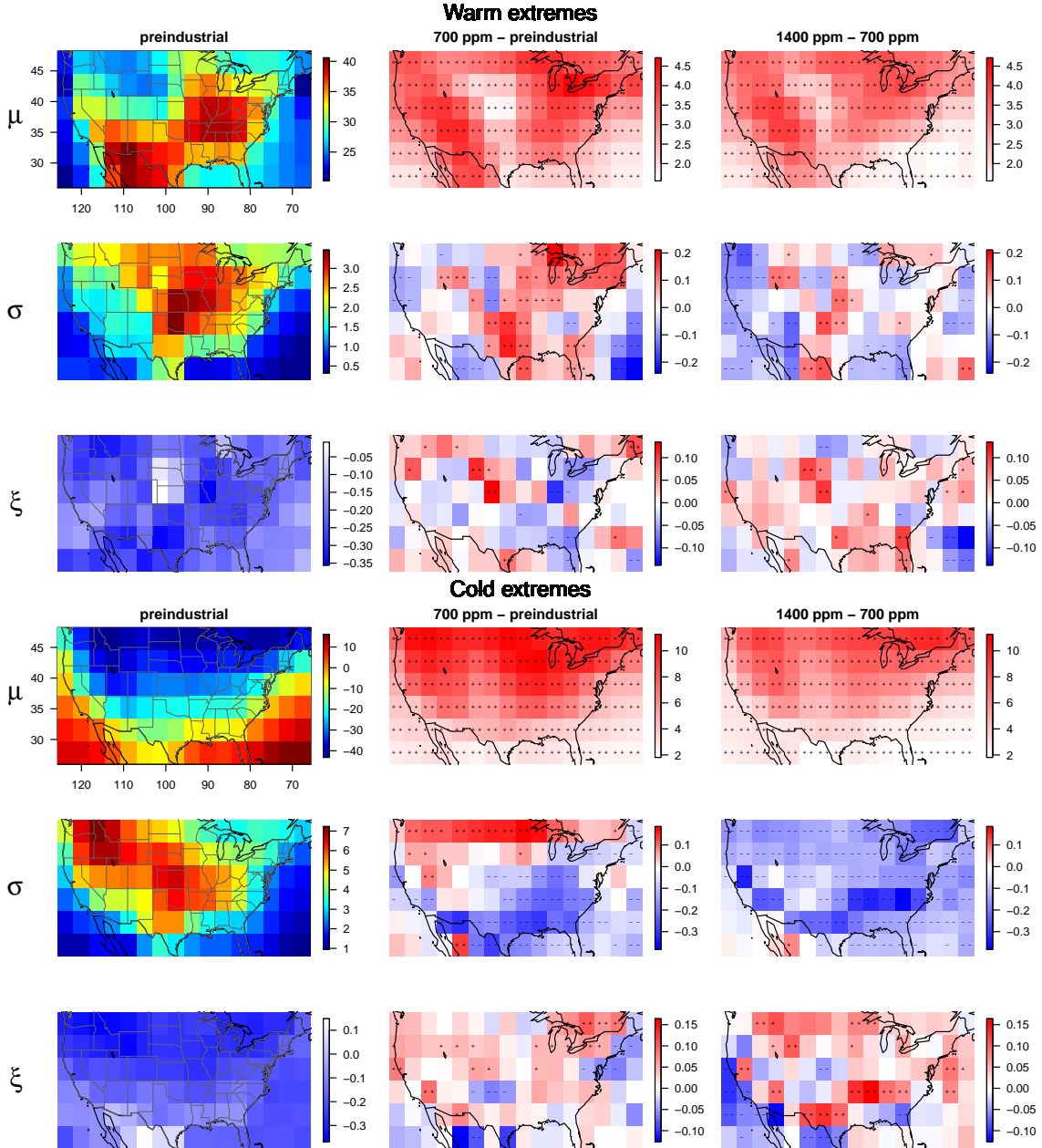


Figure 4: **Left:** Fitted GEV parameters (location  $\mu$ , scale  $\sigma$ , and shape  $\xi$ ) for seasonal extremes for the baseline model run at pre-industrial  $\text{CO}_2$  concentration. Top 3 panels are for summertime warm extremes and bottom are for wintertime cold extremes. Negative  $\xi$  is expected for temperature distributions. **Middle:** changes in parameters ( $\Delta\mu$ ,  $\Delta\log\sigma$ ,  $\Delta\xi$ ) after a warming of global mean temperature by  $3.4\text{ }^\circ\text{C}$  (by raising atmospheric  $\text{CO}_2$  to 700 ppm). **Right:** changes in parameters after an additional  $2.7\text{ }^\circ\text{C}$  warming (by raising  $\text{CO}_2$  from 700 to 1400 ppm). Grid cells with statistically significant positive or negative changes are marked with + or - symbols. (++) or (--) means the bootstrapped p-value is  $< 0.02$ ; (+ or -) means the p-value is between 0.02 and 0.10. Location parameter changes are significant, positive, and roughly linear with temperature change. Scale parameter changes at high latitudes show significant but nonlinear changes. Shape parameter changes are generally not statistically significant.

Under warmer future climate conditions, we have strong reasons to expect positive shifts in location

parameters: extremes should shift to warmer values in both summer and winter. There are however no simple physical arguments that guide expectations for changes in the scale and shape parameters. The 1000-year model runs used here allow us to accurately estimate changes in all three parameters.

Changes in the location parameters for both summer and winter extremes are, as expected, positive everywhere in the study region (Fig. 4, first and fourth rows) as climate warms. As previously found in other studies of climate model output (Kharin et al., 2007, 2013) and observations (Lee et al., 2014), the changes are asymmetric, with larger warming in winter minima than in summer maxima. For summer extremes, location parameters changes are spatially uniform and similar to changes in summer mean temperatures. For winter extremes, location parameter changes show a strong latitudinal gradient, similar in the pattern in seasonal mean changes but with greater magnitude. That is, changes in wintertime extremes exceed changes in winter means (Fig. A.8 in Appendix A.6). This asymmetry is however readily explained by the asymmetric changes in the seasonal temperature distributions. In simulated warmer climate conditions, temperature variability (the standard deviation of the distribution) is relatively unchanged in summer but strongly reduced in winter, especially at higher latitudes Holmes et al. (2015). In both summer and winter, changes in the location parameter of temperature extremes are well-explained by changes in the means and standard deviations of seasonal temperature distributions (see Fig. 5).

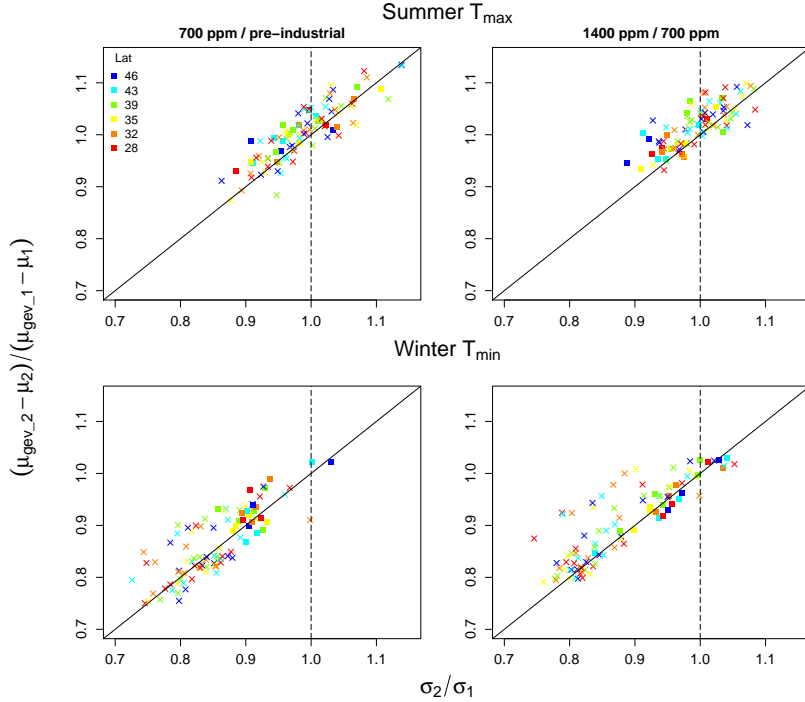


Figure 5: Test of whether location parameters for temperature extremes shift simply as expected from changes in means and standard deviations of temperature distributions. In the absence of other effects, as climate shifts from state 1 to 2, the distance between the location parameter  $\mu_{\text{gev}}$  and the overall temperature mean  $\mu$  should change according to the change in overall standard deviation  $\sigma$ , i.e.  $(\mu_{\text{gev}_2} - \mu_2) / (\mu_{\text{gev}_1} - \mu_1) = (\sigma_2 / \sigma_1)$ . Scatter plot shows these terms for all locations in study area, for summer  $T_{\text{max}}$  in upper panels and for winter  $T_{\text{min}}$  in lower panels. Left and right columns show shifts from preindustrial-700 ppm  $\text{CO}_2$  and from 700-1400 ppm  $\text{CO}_2$  climate states. Ocean locations are denoted with squares and inland locations with crosses. The closeness of points to the 1:1 line suggests that shifts in the location parameter of extremes are largely explained by changes in the overall temperature distribution. Note that from 700 to 1400 ppm  $\text{CO}_2$  climate states, the points tend to be above the line, suggesting the relationship may be more complicated for very large changes in  $\text{CO}_2$ .

In both summer and winter, scale parameters show changes that are geographically complicated but generally significant relative to pre-industrial values (see Fig. 4). For summer warm extremes, scale parameters show little change over much of the study area but modest increases over the eastern U.S., up to 20% over pre-industrial values. Scale parameters change more strongly for winter cold extremes, with a strong latitudinal gradient over land, from statistically significant decreases at lower latitudes to increases at higher latitudes. The shape parameter, in contrast, shows few statistically significant changes, other than a local region of positive shifts for winter extremes in the northern Great Lakes region.

The use of two future climate states allows us to evaluate the linearity of GEV parameters with respect to changes in mean temperature. The spatial pattern of changes in location parameters are similar in both climate transitions shown, suggesting that changes in the location parameter ( $\Delta\mu_{\text{gev}}$ ) may be approximately linear with changes in mean temperature ( $\Delta\mu$ ). We evaluate this linearity explicitly by comparing the ratio of  $\Delta\mu_{\text{gev}}/\Delta\mu$  for both climate transitions from (Fig. 6). We find that summer warm extremes do shift approximately linearly, following mean temperatures in both climate transitions. Winter cold extremes show some nonlinearity, with a latitudinal gradient. High-latitude winter extremes, which warm more strongly than the seasonal mean shift, warm still more



strongly in the warmer climate transition. That is, at high latitudes over land, the summer/winter asymmetric response of extremes appears to be amplified in warmer climate conditions. The scale parameters, by contrast, show clear nonlinear effects that are visible by eye in Fig. 4. For wintertime cold extremes, scale parameters increase at high latitude locations in the transition from preindustrial conditions to 700 ppm. For the transition from 700–1400 ppm, scale parameters decrease at these same locations, partially negating the earlier increases. Changes in both cases are statistically significant. For summertime warm extremes, the east-west difference in scale parameter behavior is preserved in both climate transitions, but more local features are not consistent in both cases. The shape parameter shows few statistically significant changes in either case.

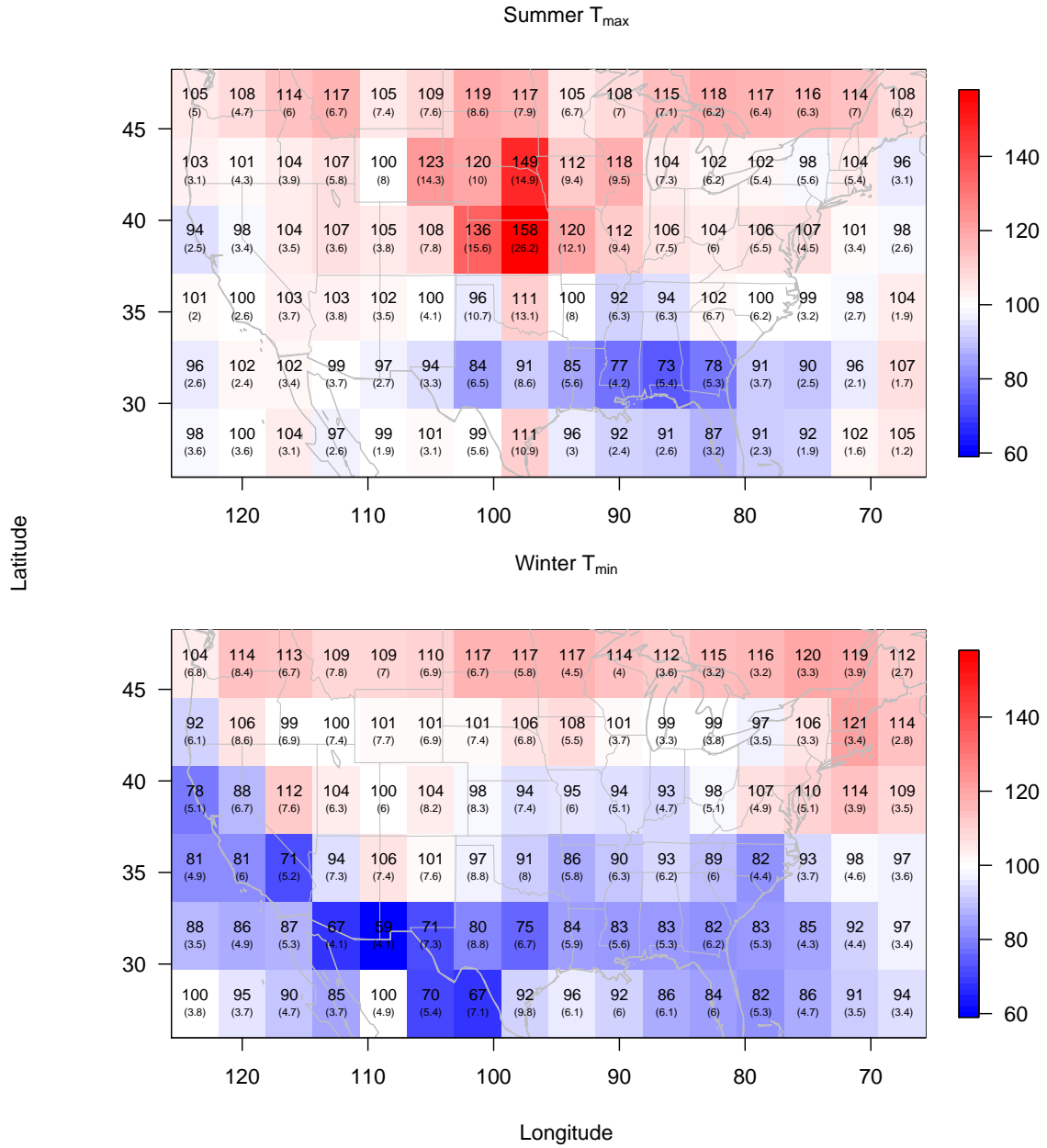


Figure 6: Test of linearity of changes in the location parameter  $\mu_{\text{gev}}$  with changes in seasonal mean temperature  $\mu$ . Colors show the ratio of  $\frac{\Delta_2 \mu_{\text{gev}}}{\Delta_2 \mu}$  to  $\frac{\Delta_1 \mu_{\text{gev}}}{\Delta_1 \mu}$ , where  $\Delta_1$  denotes the difference between the baseline climate state (289 ppm  $\text{CO}_2$ ) and that at 700 ppm  $\text{CO}_2$ , and  $\Delta_2$  denotes the difference between climate states at 700 ppm and 1400 ppm. Numbers in large font are this ratio ( $\times 100$ ); a value close to 100 indicates linearity across climate states. Numbers in parentheses and small font are the bootstrapped standard errors ( $\times 100$ ). Changes in the GEV location parameter do appear roughly linear with the increases in local seasonal mean temperatures.

## 4.2 Changes in return levels

As discussed in Section 3.2, it can be most intuitive to describe changes in tail behavior in terms of changes in return levels. We showed in Figure 3 how hypothetical changes in individual GEV parameters affect return levels at different return periods. Here we present examples of changes in the actual fitted GEV distributions of model output, and show how these produce changes in return levels. We use as examples three model locations (individual grid cells), located in Idaho (ID), California (CA), and Texas (TX) (see Fig. 2 for locations), which illustrate the behavior discussed in Section 4.1. For summer warm extremes in all three locations (Fig. 7, left columns), the changes in return levels are roughly constant for all return periods, meaning the dominant change is simply a shift in the distribution of extremes, i.e. a change in location parameter. (The TX location does show a modest increase in spread.) That shift is close to the shift in mean seasonal temperatures, as discussed previously. For winter cold extremes (Fig. 7, right columns), the scale and shape factors play a more significant role, producing return level changes that can vary with return period (though differently in different locations). Of the examples shown here, scale and shape parameters play the least significant role in the one coastal location (CA), as would be expected; the inland locations are affected more strongly.

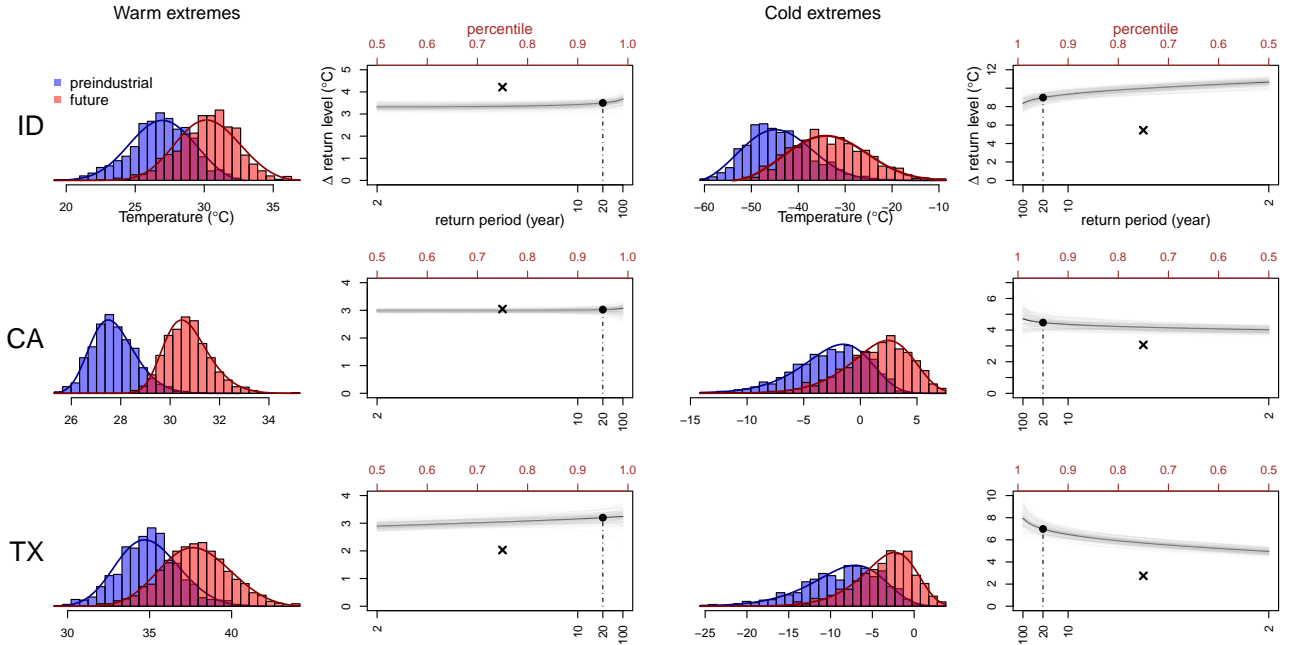


Figure 7: Illustration of the changes in return levels and their relationship with the changes in mean. Seasonal extremes changes of summer  $T_{\max}$ , winter  $T_{\min}$ , and their return levels changes (mean changes of summer  $T_{\max}$  and winter  $T_{\min}$  are marked as crosses, changes in 20-yr return levels are marked as solid circles) from preindustrial (289 ppm, blue) to future (700 ppm, red). **Top row:** Idaho pixel **Middle row:** California pixel. **Bottom row:** Texas pixel. Return levels changes for summer extremes are roughly horizontal and are close to its mean changes which implies that changes in warm extremes are mainly due to mean shift in marginal distributions. On the other hand, return levels changes for winter have three different patterns; The curve of return levels changes in the Idaho pixel shows a decreasing trend toward the lower tail. The return levels changes in the California pixel are nearly horizontal with slightly larger increase with respect to its mean changes. There is a significant increasing upward trend in the Texas pixel toward the left tail.

The asymmetric seasonal changes shown in the example locations above – summer return level changes that follow changes in means but winter return level changes that exceed them, with stronger

influence of the scale and shape parameters – are characteristic of the whole United States region. Figures 8 and 9 show the changes in return levels across return periods from 2 to 100 years, for summer and winter extremes, respectively. For summer extremes, changes in return levels are relatively flat, implying that the dominant effect is a change in the location parameter. Exceptions include a small part of the central Midwest corn belt region and the far Northeast, which show increases in return levels with return periods. The sharply rising “extreme extremes” in a few Midwest locations is due to strong and statistically significant changes in the shape parameter (but see the equivalent figure for annual maxima in Fig. A.4 in Appendix A.2, the sharply rising pattern is less pronounced); these effects grow still further in the transition to a 1400 ppm climate (Fig. A.9 in Appendix A.7 ). For winter extremes, return level changes for ocean locations are flat, but inland locations tend to show striking effects of changes in scale and shape parameters. For the transition to a 700 ppm climate, at low latitudes, return levels increase as the return period increases, exacerbating the “extreme extremes”, but at high latitudes, the pattern reverses, and return levels decrease as the return period increases. Because of the aforementioned nonlinearity in the evolution of the scale parameter for winter extremes, these high-latitude effects partially reverse as CO<sub>2</sub> levels are raised to 1400 ppm (Fig. A.9 in Appendix A.7).

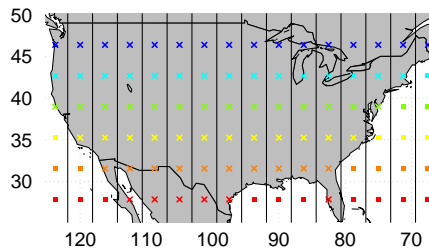
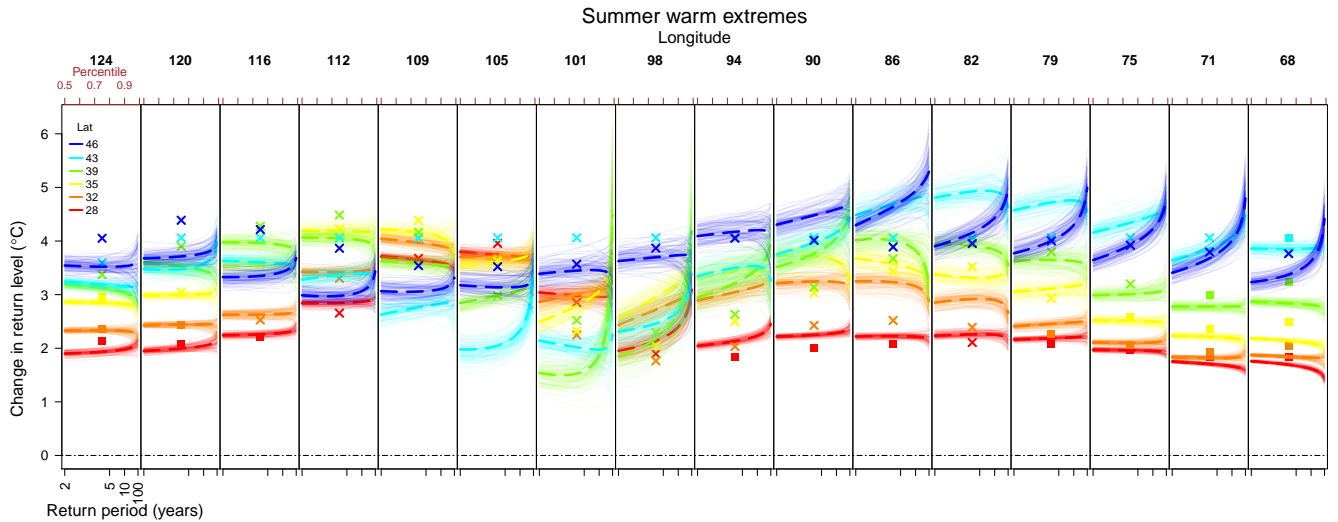


Figure 8: Estimated changes in return levels of summer  $T_{\max}$  for future (700 ppm  $\text{CO}_2$ ) vs. past (289 ppm  $\text{CO}_2$ ) climate states, for all 96 grid cells in the study area. Each panel shows results from the 6 grid cells in a longitude band, with each color represents a latitude band, as shown in the small map below. The horizontal axis for each panel is the return period, and estimated changes in return levels are plotted in their correspondingly colored thick dashed lines. Estimates obtained from block bootstrapped samples by resampling years are plotted to form envelopes representing the associated uncertainties. The corresponding mean change for each grid cell is marked as a cross symbol for inland locations and filled box for ocean locations. Note that for most locations (except the Northeast and a few grid cells in the Midwest), the curves of return levels changes are fairly flat, meaning the changes are largely due to changes in the location parameter. Furthermore, the return level changes are close to their corresponding mean temperature changes, implying that changes in extremes are due to a simple shift of the whole distribution of daily temperatures. The sharply rising pattern in three Midwest locations is diminished if one uses annual maxima.

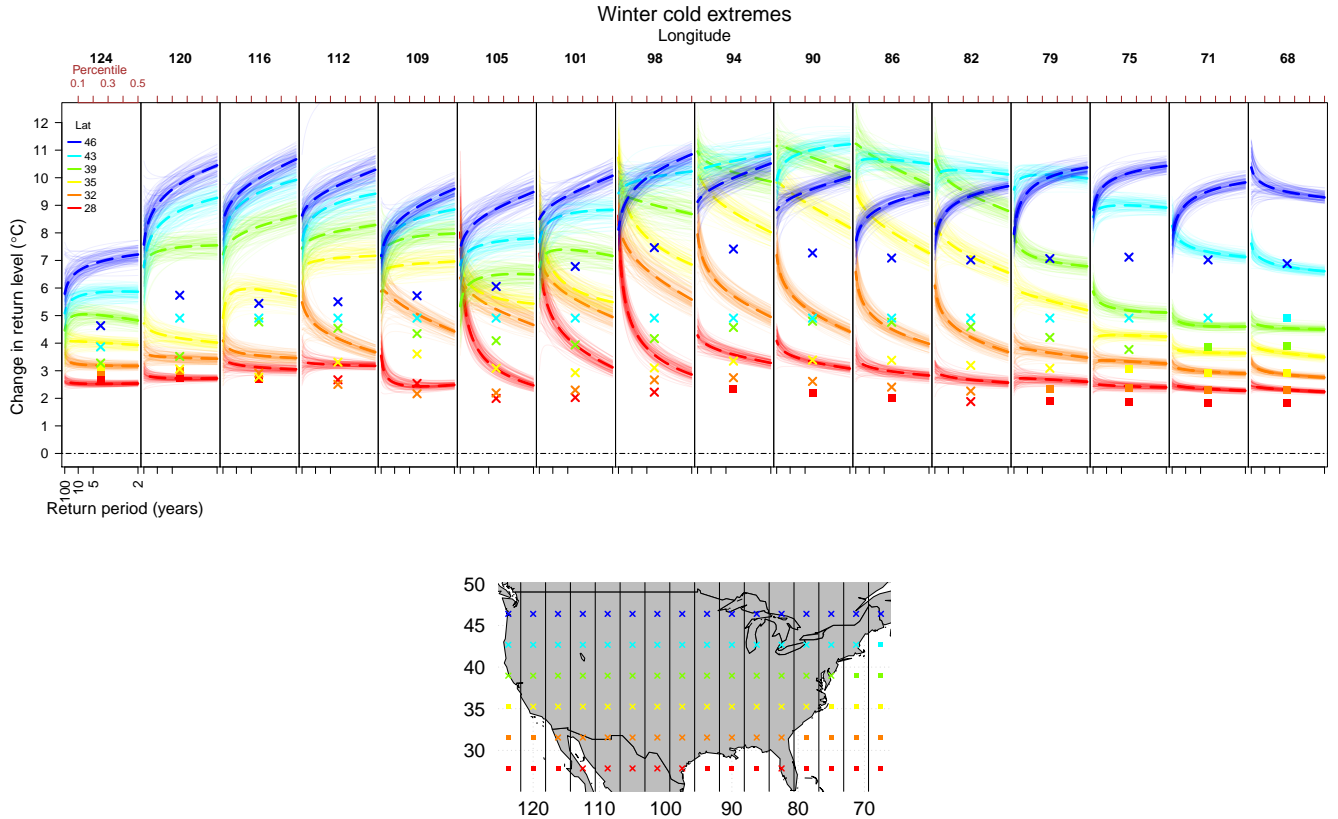


Figure 9: As in Fig. 8 but for winter  $T_{\min}$ . (Note that the return period axis is now flipped so that longer return periods are on the left.) In general, cold extremes warm more than do means, especially at high latitudes. In the inland Southwest and South, changes in return levels show an upward curving pattern, meaning that warming is stronger for the colder winters. In all high-latitude inland locations, changes in return levels show a downward curving pattern, meaning that warming is weaker for the colder winters. These effects are driven by decreases and increases, respectively, in the scale or shape parameters.

## 5 Sensitivity analysis: GEV block size

In this analysis, as in many climate applications of EVT, we have assumed that the seasonal block is long enough that the GEV distribution is approximately valid. Our long time series allows us to explicitly test this assumption. The test relies on the fact that the GEV distribution has the property of “max-stability”. In the context of distributions of block maxima ( $M_n$ ), max-stability means that the distribution after normalization is identical for any block size larger than  $n$ .

In our case, if the seasonal block is long enough that the GEV distribution is approximately valid for a given time series, then the shape parameter estimate  $\hat{\xi}_n$  obtained with seasonal blocks should be approximately the same as that obtained with a larger block size  $n'$  ( $\hat{\xi}_{n'}$ ). The validity of the GEV approximation using seasonal extremes can therefore be assessed by checking the consistency of estimated shape parameters using longer block sizes.

We refit GEV distributions for each pixel in our study region with block maxima/minima taken over 2, 5 and 10 years, and compare shape parameters. We find that for summer maxima, the differences in  $\xi$  with block size are distributed around zero, suggesting that a seasonal block size may be sufficient (Fig. 10, upper right panel). For winter minima, we see effects of block size with latitudinal structure:

longer blocks produce larger  $\xi$  at high latitudes, where changes in extremes are largest (Fig. 10, upper left panel). These results suggest that single seasons may not be sufficiently long for the GEV approximation to be accurate.

These results also suggest that quantile–quantile plots (see Fig. A.6 in Appendix A.4) may not be a sufficient test of the appropriateness of the GEV distribution. However, we also find that use of seasonal blocks may be sufficient for estimating *changes* in the shape parameter across climate states. Even if biases related to block length exist, if they are consistent in different climate states, then use of seasonal extremes would not compromise analysis of changes in GEV distributions. We do in fact find that differences in estimated shape parameters for different climate states are relatively stable across different block sizes, for both summer and winter extremes (Fig. 10, lower panels).

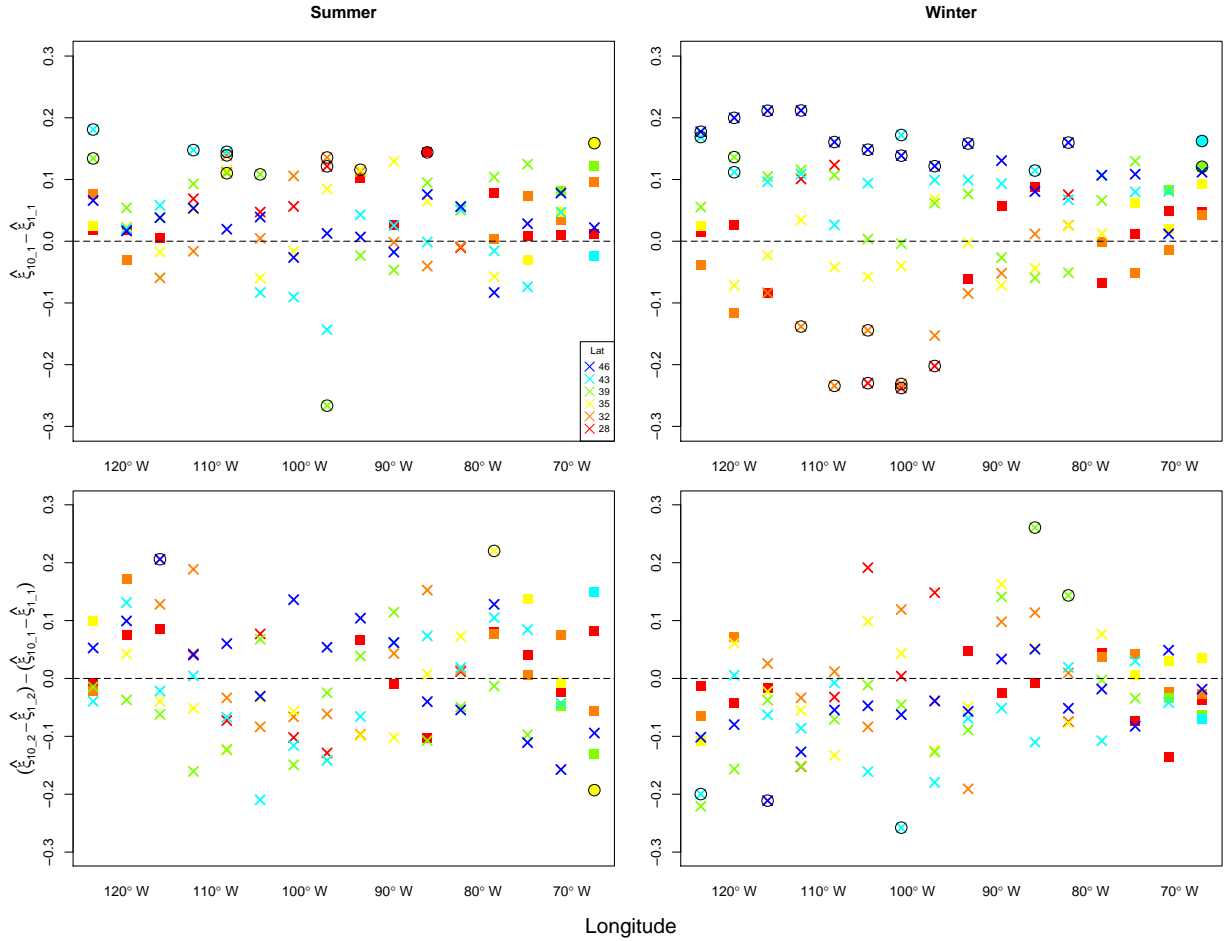


Figure 10: **Upper** panels: differences in estimated shape parameters for summer warm (**left**) and winter cold (**right**) extremes, obtained using different block sizes (1- vs. 10-year blocks). Estimates are shown are those for the pre-industrial climate state, for all model grid cell locations in the study area, with the same color and symbol scheme as in previous figures. (Subscripts in notation denote the climate state and block length, e.g.  $\hat{\xi}_{10\_1}$  means 10-year blocks and climate state 1, i.e. pre-industrial.) Circled datapoints are those locations where differences in estimates of shape parameter changes are significant at the 0.05 level. For summer extremes, differences in estimates obtained with different block sizes are distributed around zero (horizontal dashed line) for all locations. For winter extremes, differences show latitude-dependent biases, with systematic positive deviations from the reference line for most high-latitude locations (10-year blocks produce higher values) and negative deviations for low-latitude western inland locations (10-year blocks produce lower values). These results suggest that for cold extremes, in some areas seasonal blocks may be insufficiently long for the GEV approximation to be valid. **Lower** panels: differences in estimates of *changes* in shape parameters across pre-industrial and high-CO<sub>2</sub> (700 ppm) climates obtained with 1- vs. 10-year blocks. Differences are distributed around zero with no latitudinal structure. These results may imply that seasonal blocks are sufficiently long for investigating *changes* in the shape parameter across different climate states.

## 6 Sensitivity analysis: data length on return level estimation

The thousand-year model runs used in this work provide fairly accurate estimates of changes in return levels even for long return periods. Estimated uncertainties on return level changes – the bootstrapped



envelopes in Fig. 9 – are generally within 20% of the estimated changes even for 100-year return periods. This dataset therefore allows us to study empirically how well GEV methods work when applied to model output at the shorter lengths (decades to centuries) more commonly used in climate studies.

To test how uncertainties increase with shorter model runs, we divide the time series into segments of 20 and 50 years and refit the GEV parameters for each segment. The resulting distributions of estimates for summer and winter extremes are shown in Figures 11 and 12.

The results show that sampling error can be large when using climate simulations of length comparable to the return periods of interest. In both summer and winter, the distribution of estimates of return level changes derived from short model segments are centered around their “true” values but with large spread (Fig. 11 and 12). In these examples, the sampling errors are comparable to their “true” changes in return level when 20-year segments are used. Unsurprisingly, spreads are largest when using short model segments to predict long return periods. For example, for the Idaho test location, when changes in wintertime 100-year return levels are estimated using 20-year segments (Fig. 12 lower left panel), those estimates can differ by  $\pm 10^\circ\text{C}$  while the “true” change is only  $8.3^\circ\text{C}$ . Because sampling errors can be large with only 20 data points (see Fig. 13), the 20-year segments also occasionally lead to highly unreliable estimates of return level changes driven by poor estimates of the shape parameter (Katz et al., 2002). One case of this is highlighted in Figure 12: a single 20-year segment produces pathological estimates of return level changes in two of the three test pixels. (See Fig. 3 for illustration of how the shape parameter affects estimated return levels.)

The example locations shown in Figures 11 and 12 are representative of land locations in the entire study area. In Figure 13 we show the spread in estimates for all model grid cells when estimating changes in 20-year returns (both summer and winter) with 20-year segments and changes in 50-year returns with 50-year segments. For inland locations, the spread in estimates is comparable to the true change for the 20-year case but somewhat lower for the 50-year case. The length of the model segment is especially important for temperature extremes, because their distribution has a bounded tail. Ocean locations show much smaller sampling error, presumably because changes in extremes are produced predominantly by shifts in the location parameter and not the scale or shape parameters, which are more difficult to estimate. The locations with largest uncertainties are indeed those with the largest changes in shape parameter: a few Midwest locations for warm extremes and some locations in Mexico for cold extremes.

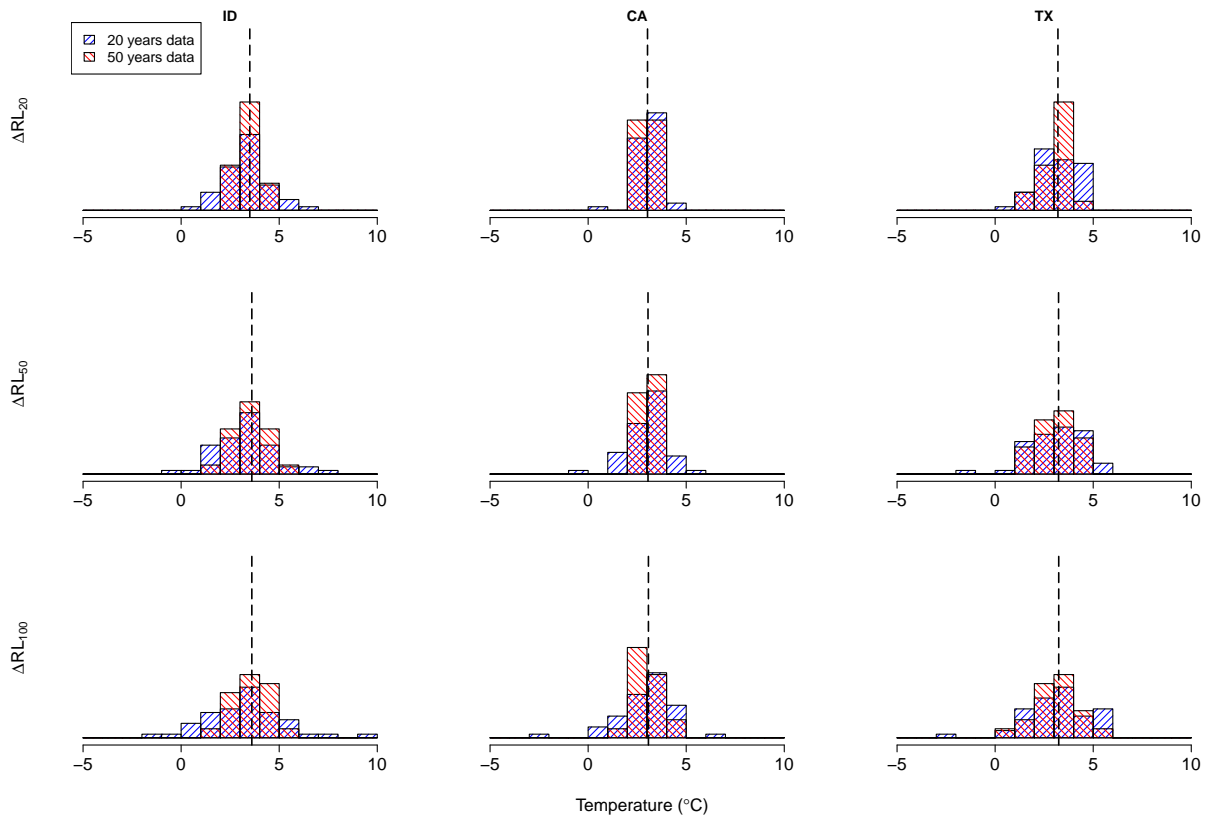


Figure 11: Estimates of changes in return levels (20, 50, 100 year return periods) obtained by using different length segments (20 and 50 years, shown as blue and red histograms), as compared to the “ground-truth” changes obtained with the full 1000-year run (dashed lines). We show summer warm extremes for the same three pixels shown in previous figures, located in Idaho, California, and Texas. Pre-industrial return levels for these locations (for 20, 50, and 100 year periods) are ID: 30.40, 31.09, and 31.49  $^{\circ}\text{C}$ ; CA: 29.34, 29.80, and 30.11  $^{\circ}\text{C}$ , and TX: 38.12, 38.89, and 39.36  $^{\circ}\text{C}$ .

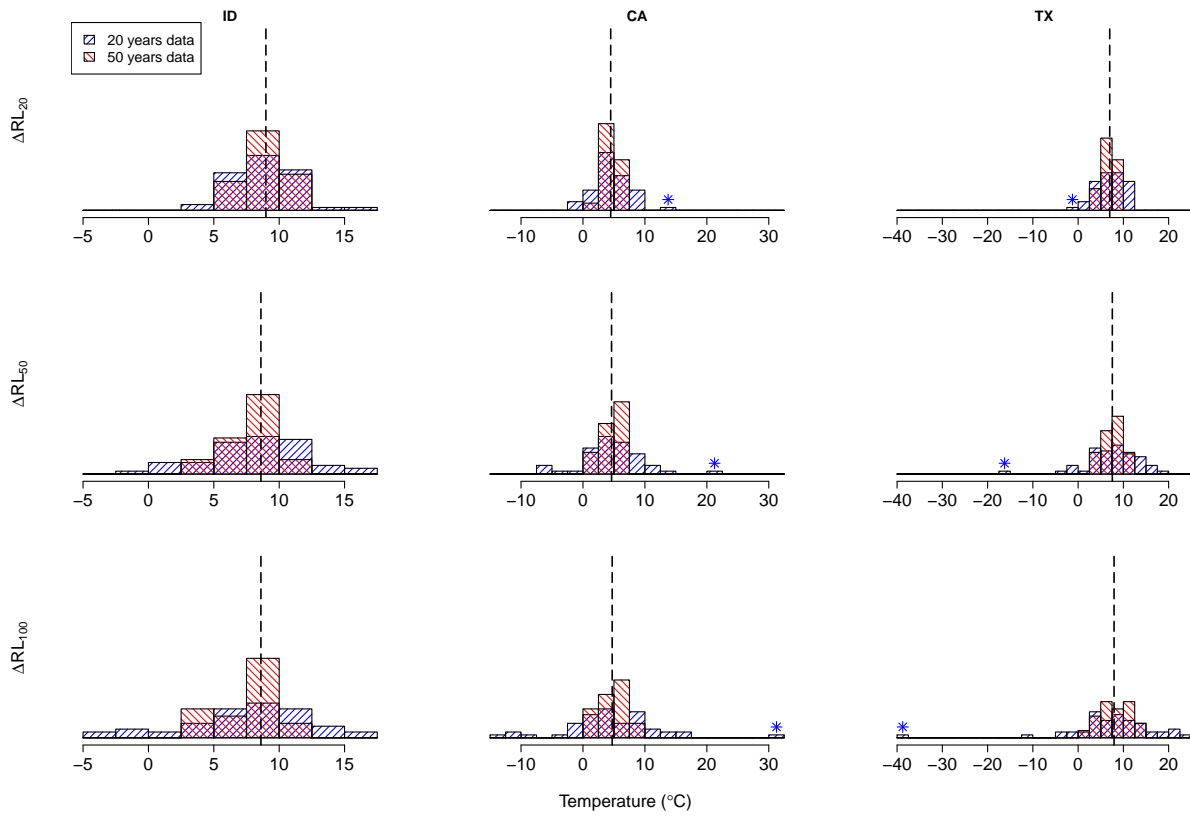


Figure 12: As in Figures 11 but for winter cold extremes. Pre-industrial return levels for these locations are ID: -54.87, -56.78, and -57.83 °C; CA: -8.49, -10.38, and -11.70 °C, and TX: -17.22, -20.02, and -21.98 °C. Especially unreliable estimates of return levels were obtained for one 20-year period in CA and TX respectively (denoted by \*), these parameter estimates are mainly due to the unreliable estimates of the shape parameter (off by -0.91 in CA and 0.75 in TX) for those particular 20 years data.

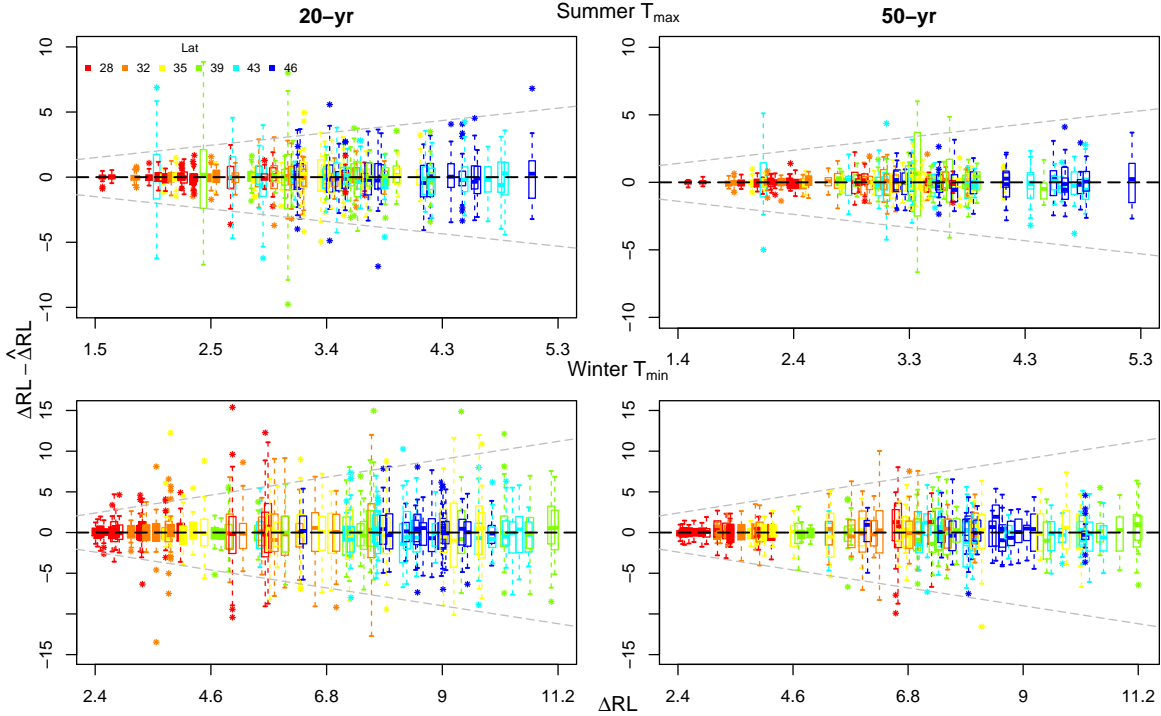


Figure 13: Sampling errors in estimates of return level changes induced by using short data segments, for all model grid cells in the study area. Values shown are the estimated return level change minus the “ground-truth” change determined from the entire 1000-year segment ( $\Delta\text{RL} - \hat{\Delta\text{RL}}$ ), plotted against the “ground-truth” change. Left: distribution of estimates of changes in 20-year return levels made using 20-year segments. Right: the same for 50-year return levels and 50-year segments. Top and bottom rows show summer and winter extremes. Filled boxes are ocean locations and unfilled are land. For each location, the median estimate is marked with a band and the box encloses the middle 50% of estimates, i.e. top and bottom edges mark the first (Q1) and third (Q3) quartiles. Whiskers extend to the lowest (highest) estimate that falls within 1.5 box lengths ( $Q3 - Q1$ ) of those edges. (If the distribution were normal, whiskers would extend to  $\pm 2.7\sigma$ .) Remaining outliers are marked with circles. Gray reference lines are the 1:1 lines (i.e. sampling error = return level change). For most inland locations, the estimation uncertainty is close to the magnitude of return level change (i.e. whiskers are close to reference lines). Ocean locations show smaller changes but also smaller effects of sampling error. The three cases of anomalously large uncertainty for summer extremes are those Midwest locations whose annual maxima are do not reliably occur in JJA, discussed in Section 2. As expected, relative uncertainties decrease when using 50-year segments (results not shown).

It is worth noting that the limitations of short model runs can be overcome with ensembles of statistically independent runs. And in cases where only a single run is available, spatial modeling approaches may also be able to reduce estimation variability (see further discussion in following section). In the absence of such approaches, however, this assessment suggests that when using single model runs, sampling error may be significant when the length of the climate simulation is comparable to the return period of interest.

## 7 Discussion

In this study we use extreme value theory to study changing temperature extremes in model projections of future climate states. Following prior work, we assume the GEV model provides a reasonable

approximation for the distribution of seasonal temperature extremes (see Fig 7) and that changing temperature extremes can therefore be studied by estimating changes in GEV parameters and resulting implied changes in return levels. We use millennial-scale equilibrated simulations of pre-industrial and higher-CO<sub>2</sub> conditions (producing changes in global mean temperature of 3.4 and 6.1°C) to explore both the physics of climate model projections and the utility of statistical approaches based on GEV distributions in different contexts.

Our results suggest that for the U.S. area, much of the behavior of temperature extremes in higher CO<sub>2</sub> climate states appears a straightforward result of changes in underlying temperature distributions. Summertime warm extremes generally shift simply in accordance with mean shifts in summer temperatures. Winter time cold extremes warm more strongly than do winter mean temperatures, but largely do so as expected given decreased variability in wintertime temperatures. In both cases, the changes in the location parameter of extremes appear well-explained by shifts in overall temperature means and variability (see Fig. 5). Comparison across climate simulations also suggests that these changes are roughly linear with the increase in local seasonal mean temperatures (Fig. 6). In some locations, however, especially inland locations in the winter, changes in the scale and shape parameters do provide an additional complication, producing substantial differences in return level changes at different return periods (Fig. 9).

The millennial-scale model runs also allow us to assess the validity of the use of annual or seasonal block sizes in studies of GEV distributions of temperature extremes. Our results suggest that blocks of individual seasons are sufficiently long for representing summer warm extremes, but may be insufficient for cold extremes, especially for inland locations at high latitudes. In these locations altering the block length alters the shape parameter of the estimated GEV distribution (Fig. 10 upper panel). We observe however that seasonal blocks may be long enough for the study of the *changes* of extremes (Fig. 10 lower panel). Changes in shape parameter are more consistent with block length, suggesting that potential biases related to block length may be consistent in different climate states. In general, increasing block size reduces biases, but can increase sampling error in estimates if the time series is limited. Choice of block size therefore requires consideration of inherent tradeoffs.

It is important to note that regardless of whether seasonal (90-92 days) or annual (365 days) extremes are used, the effective block size is still smaller, as most annual extremes fall into a restricted part of the year. For inland locations, the interquartile range (IQR) of the distribution of the timing of annual extremes is usually 30-40 days; for oceans it can be 60 days, especially in winter (Fig. A.3). Block size limitations can therefore be more significant than they may seem on first glance.

The basic motivation for using seasonal rather than annual extremes is that the assumption of independent and identically distributed data is likely more valid for an individual season than for an entire year. In temperature extremes, the distinction between annual and seasonal extremes in the U.S. region appears generally insignificant. In most inland locations, the distribution of the timing of annual extremes is largely confined to the expected season (summer, JJA or winter, DJF, see Fig. A.3). As a result, estimated GEV distributions and changes in return levels are almost identical regardless of whether seasonal or annual extremes are used (see Fig. A.4). However, in some Midwest locations this practice produces artifacts (see Fig. 8): significant fractions ( $\approx 40\%$ ) of annual maxima fall outside summer (see Fig. A.2 (d) and Fig. A.3). In some ocean locations, annual maxima and minima fall in narrow time windows but ones that lie outside the expected seasons (Fig. A.2 and A.3). For temperature extremes, it is reasonable to consider both seasonal or annual extremes. Which is more relevant may depend on the application; for example, for agricultural impacts, extremes during a growing season will be more relevant than an annual extreme.

The long runs used here also enable detailed investigation of the relationships of data length and GEV sampling error. Over inland locations, estimation uncertainty can be significant when using climate simulations of length comparable to the return periods of interest (Fig. 13). Ocean locations show much smaller sampling error, presumably because changes in extremes are dominated by shifts in their distribution, whose spread and shape does not otherwise change significantly. The sampling

error can become prohibitively large when using short model segments (e.g. 20 years) to extrapolate long return periods (see Fig. 12). Extrapolation should be carried out with caution (as also noted by Kharin et al. (2007)). Even when the length of a model run is comparable to the return period of interest, our results suggest that resulting estimates may show large uncertainty, especially for runs of only 20 years length.

While this analysis benefits from the use of millennial-scale simulations, the requirement of simulation length restricts us to examining a single climate model, run at fairly coarse resolution. A single model provides an insufficient guide for understanding how temperature extremes may change in future climate conditions. However, looking across different climate models is complicated by the fact that the multi-model comparison data available in publicly available archives are not ideal for estimating changes in extremes. The length of the runs are much shorter than those we have in this study ( $\approx 100$  years); the number of runs for any scenario is small; and climate conditions in the simulations are evolving rather than stationary. Estimating GEV distributions that are changing over time is even more challenging than in the equilibrium setting, making the limitations of short model runs even more significant. If understanding changes in extremes is a research priority, larger ensembles of model runs would be helpful.

In the absence of large ensembles, one could potentially overcome some of the limitations of restricted data by exploiting the spatial structure of temperature extremes (see Fig. 4) to “borrow the strength over space”. Numerous prior studies do explicitly model the spatial structure of a climate variable of interest, e.g. Cooley et al. (2007); Cooley and Sain (2010); Craigmile et al. (2013); Wang et al. (2015). We do not use these approaches in this work since the millennial-scale model runs allow us to estimate the GEV parameters and their changes accurately, and spatial modeling is not ideal: it may introduce bias and greatly complicates the computation. However, in cases where only shorter time series (decades to centuries) of model runs or observations are available, appropriate spatial modeling may be essential to reduce estimation uncertainty.

Extreme value theory (EVT) has become a popular approach for studying climate extremes. However, one should be aware of the underlying assumptions, the corresponding implications, and the potential limitations when applying it. EVT can potentially allow characterizing tail behavior that differs from that of the underlying distribution, but it involves a corresponding penalty, as fitting a distribution of block extremes necessarily involves throwing out most of one’s data. For short time series, care must be taken to ensure that the drawbacks do not outweigh the benefits. In the climate model output studied here, for example, shifts in the location parameter for both summer and winter extremes are well-explained by changes in the underlying temperature distribution. With millennial time series we can also identify significant changes in the scale parameter, especially for winter extremes. With shorter time series, sampling error that degrades estimation of the return levels can negate any benefits of EVT. While EVT is a powerful tool, long model runs such as those used here are essential for understanding the contexts in which it should best be used in studying climate extremes, and for devising approaches for working with shorter model time series or observational datasets.

## Acknowledgements

This work was conducted as part of the Research Network for Statistical Methods for Atmospheric and Oceanic Sciences (STATMOS), supported by NSF Award #s 1106862, 1106974, and 1107046, and the Center for Robust Decision Making on Climate and Energy Policy (RDCEP), supported by the NSF Decision Making Under Uncertainty program Award # 0951576.

## References

L. Alexander, X. Zhang, T. Peterson, J. Caesar, B. Gleason, A. Klein Tank, M. Haylock, D. Collins, B. Trewin, F. Rahimzadeh, et al. Global observed changes in daily climate extremes of temperature

- and precipitation. *Journal of Geophysical Research: Atmospheres (1984–2012)*, 111(D5), 2006.
- J. Beirlant, Y. Goegebeur, J. Segers, and J. Teugels. *Statistics of extremes: theory and applications*. John Wiley & Sons, 2004.
- S. Castruccio, D. J. McInerney, M. L. Stein, F. Liu Crouch, R. L. Jacob, and E. J. Moyer. Statistical emulation of climate model projections based on precomputed gcm runs\*. *Journal of Climate*, 27(5):1829–1844, 2014.
- S. Coles, J. Bawa, L. Trenner, and P. Dorazio. *An introduction to statistical modeling of extreme values*, volume 208. Springer, 2001.
- W. D. Collins, C. M. Bitz, M. L. Blackmon, G. B. Bonan, C. S. Bretherton, J. A. Carton, P. Chang, S. C. Doney, J. J. Hack, T. B. Henderson, et al. The community climate system model version 3 (ccsm3). *Journal of Climate*, 19(11):2122–2143, 2006.
- D. Cooley and S. R. Sain. Spatial hierarchical modeling of precipitation extremes from a regional climate model. *Journal of agricultural, biological, and environmental statistics*, 15(3):381–402, 2010.
- D. Cooley, D. Nychka, and P. Naveau. Bayesian spatial modeling of extreme precipitation return levels. *Journal of the American Statistical Association*, 102(479):824–840, 2007.
- P. F. Craigmile, P. eter Guttorp, et al. Can a regional climate model reproduce observed extreme temperatures? *Statistica*, 73(1):103–122, 2013.
- A. C. Davison and R. L. Smith. Models for exceedances over high thresholds. *Journal of the Royal Statistical Society. Series B (Methodological)*, pages 393–442, 1990.
- L. de Haan and A. Ferreira. *Extreme value theory: an introduction*. Springer, 2006.
- D. R. Easterling, G. A. Meehl, C. Parmesan, S. A. Changnon, T. R. Karl, and L. O. Mearns. Climate extremes: observations, modeling, and impacts. *science*, 289(5487):2068–2074, 2000.
- B. Efron. Bootstrap methods: another look at the jackknife. *The annals of Statistics*, pages 1–26, 1979.
- J. H. Einmahl, L. Haan, and C. Zhou. Statistics of heteroscedastic extremes. *Journal of the Royal Statistical Society: Series B (Statistical Methodology)*, 2015.
- R. A. Fisher and L. H. C. Tippett. Limiting forms of the frequency distribution of the largest or smallest member of a sample. In *Mathematical Proceedings of the Cambridge Philosophical Society*, volume 24, pages 180–190. Cambridge Univ Press, 1928.
- M. D. Frías, R. Mínguez, J. M. Gutiérrez, and F. J. Méndez. Future regional projections of extreme temperatures in europe: a nonstationary seasonal approach. *Climatic change*, 113(2):371–392, 2012.
- P. Frich, L. Alexander, P. Della-Marta, B. Gleason, M. Haylock, A. Klein Tank, and T. Peterson. Observed coherent changes in climatic extremes during the second half of the twentieth century. *Climate Research*, 19(3):193–212, 2002.
- B. Gnedenko. Sur la distribution limite du terme maximum d’une serie aleatoire. *Annals of mathematics*, pages 423–453, 1943.
- E. J. Gumbel. *Statistics of extremes*. 1958.
- C. R. Holmes, T. Woollings, E. Hawkins, and H. de Vries. Robust future changes in temperature variability under greenhouse gas forcing and the relationship with thermal advection. *Journal of Climate*, (2015), 2015.

- T. Hsing. On tail index estimation using dependent data. *The Annals of Statistics*, pages 1547–1569, 1991.
- . IPCC. *Climate change 2013: The physical science basis*. Cambridge University Press Cambridge, UK, and New York, 2014.
- R. W. Katz, M. B. Parlange, and P. Naveau. Statistics of extremes in hydrology. *Advances in water resources*, 25(8):1287–1304, 2002.
- V. V. Kharin and F. W. Zwiers. Changes in the extremes in an ensemble of transient climate simulations with a coupled atmosphere-ocean gcm. *Journal of Climate*, 13(21):3760–3788, 2000.
- V. V. Kharin and F. W. Zwiers. Estimating extremes in transient climate change simulations. *Journal of Climate*, 18(8):1156–1173, 2005.
- V. V. Kharin, F. W. Zwiers, X. Zhang, and G. C. Hegerl. Changes in temperature and precipitation extremes in the ipcc ensemble of global coupled model simulations. *Journal of Climate*, 20(8):1419–1444, 2007.
- V. V. Kharin, F. Zwiers, X. Zhang, and M. Wehner. Changes in temperature and precipitation extremes in the cmi5 ensemble. *Climatic Change*, 119(2):345–357, 2013.
- K. E. Kunkel, R. A. Pielke Jr, and S. A. Changnon. Temporal fluctuations in weather and climate extremes that cause economic and human health impacts: A review. *Bulletin of the American Meteorological Society*, 80(6):1077–1098, 1999.
- H. R. Künsch. The jackknife and the bootstrap for general stationary observations. *The Annals of Statistics*, pages 1217–1241, 1989.
- M. R. Leadbetter, G. Lindgren, and H. Rootzén. Extremes and related properties of random sequences and processes. *Springer Series in Statistics*, 1983.
- J. Lee, S. Li, and R. Lund. Trends in extreme us temperatures. *Journal of Climate*, 27(11):4209–4225, 2014.
- W. B. Leeds, E. J. Moyer, and M. L. Stein. Simulation of future climate under changing temporal covariance structures. *Advances in Statistical Climatology Meteorology and Oceanography*, 1(1):1–14, 2015. doi: 10.5194/ascmo-1-1-2015. URL <http://www.adv-stat-clim-meteorol-oceanogr.net/1/1/2015/>.
- P. Naveau, A. Guillou, and T. Rietsch. A non-parametric entropy-based approach to detect changes in climate extremes. *Journal of the Royal Statistical Society: Series B (Statistical Methodology)*, 76(5):861–884, 2014.
- NOAA. Billion-dollar weather and climate disasters: Overview. <https://www.ncdc.noaa.gov/billions/>, 2015.
- J. Pickands III. Statistical inference using extreme order statistics. *the Annals of Statistics*, pages 119–131, 1975.
- S. I. Resnick. *Extreme values, regular variation, and point processes*. Springer, 1987.
- S. I. Resnick. *Heavy-tail phenomena: probabilistic and statistical modeling*. Springer, 2007.
- B. A. Shaby and B. J. Reich. Bayesian spatial extreme value analysis to assess the changing risk of concurrent high temperatures across large portions of european cropland. *Environmetrics*, 23(8):638–648, 2012.



- A. B. Smith and R. W. Katz. Us billion-dollar weather and climate disasters: data sources, trends, accuracy and biases. *Natural hazards*, 67(2):387–410, 2013.
- R. L. Smith. Extreme value analysis of environmental time series: an application to trend detection in ground-level ozone. *Statistical Science*, pages 367–377, 1989.
- A. Stephenson and J. Heffernan. ismev: An introduction to statistical modeling of extreme values. *R package version*, 1, 2012.
- A. Sterl, C. Severijns, H. Dijkstra, W. Hazeleger, G. Jan van Oldenborgh, M. van den Broeke, G. Burgers, B. van den Hurk, P. Jan van Leeuwen, and P. van Velthoven. When can we expect extremely high surface temperatures? *Geophysical Research Letters*, 35(14), 2008.
- C. Tebaldi, K. Hayhoe, J. M. Arblaster, and G. A. Meehl. Going to the extremes. *Climatic change*, 79(3-4):185–211, 2006.
- J. Wang, Y. Han, M. L. Stein, V. R. Kotamarthi, and W. K. Huang. Evaluation of dynamically downscaled extreme temperature using a generalized extreme value (gev) model. *Climate Dynamics*, under review, 2015.
- S. Westra, L. V. Alexander, and F. W. Zwiers. Global increasing trends in annual maximum daily precipitation. *Journal of Climate*, 26(11):3904–3918, 2013.
- S. G. Yeager, C. A. Shields, W. G. Large, and J. J. Hack. The low-resolution ccsm3. *Journal of Climate*, 19(11):2545–2566, 2006.
- F. W. Zwiers and V. V. Kharin. Changes in the extremes of the climate simulated by ccc gcm2 under co2 doubling. *Journal of Climate*, 11(9):2200–2222, 1998.

## A.1 Comparison of distribution of extremes with overall distribution: summer

In this appendix, we show the comparison of the overall distribution and the distribution of extremes, as in Fig. 1 but here for summer rather than winter.

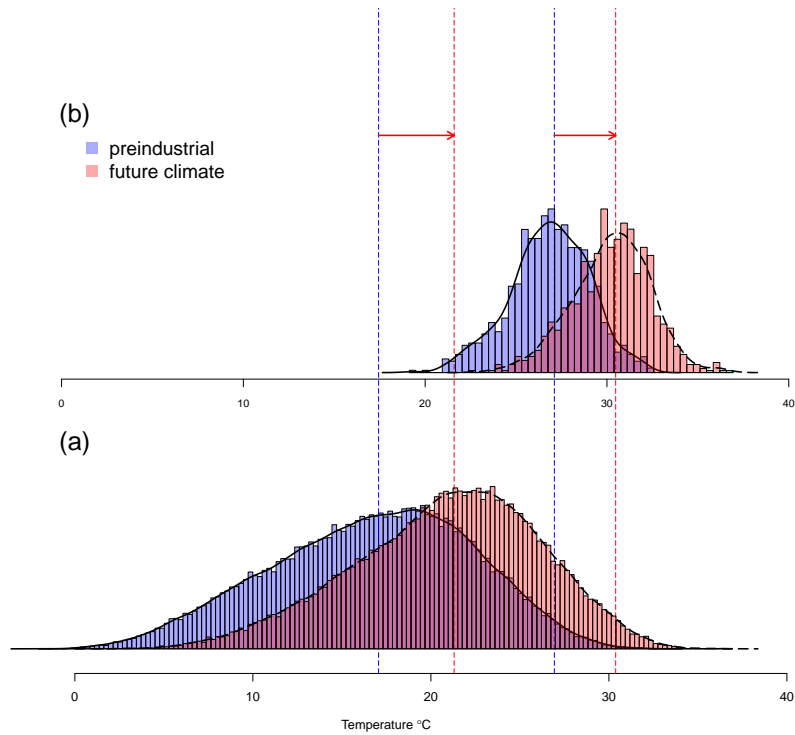


Figure A.1: As in Figure 1 but for summer warm extremes. **(a)** Overall distribution of summer (JJA) daily maximum temperature ( $T_{\max}$ ) in a north Idaho location, for baseline and 700 ppm  $\text{CO}_2$  climate states. **(b)**: distributions of seasonal maxima of summer  $T_{\max}$ . Note that the median shift of the overall distribution is now slightly larger than that of the distribution of extremes; the opposite was true for winter cold extremes.

## A.2 Annual extremes vs. seasonal extremes

In this work, we use seasonal extremes (i.e. summer (JJA) warm extremes and winter (DJF) cold extremes) instead of the annual warm/cold extremes. Most of the time, the annual extremes and seasonal extremes coincide (see Fig. A.3). As a result, there is little difference between the GEV results by using annual extremes and seasonal extremes.

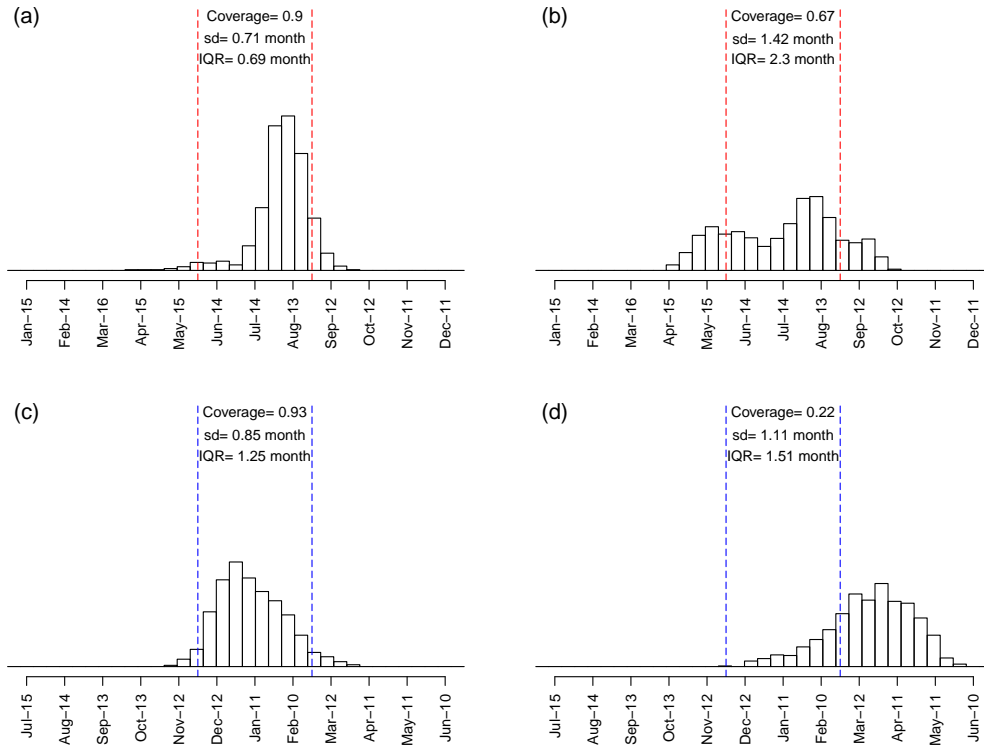


Figure A.2: Histograms of the timing when annual extremes (maxima (**upper**), minima (**lower**)) occurs. **Left:** (a) and (c) are histograms for the example locations in TX and ID, respectively, used throughout the manuscript. They show the general pattern of annual maxima in JJA and minima in DJF. **Right:** (b) a Midwest location (Lon: 101 Lat: 39 ) where the use of summer maxima is problematic: 33% of annual maxima fall outside JJA. (d) An ocean location (Lon: 124 Lat: 28) that shows a delay of coldest temperatures until after DJF.

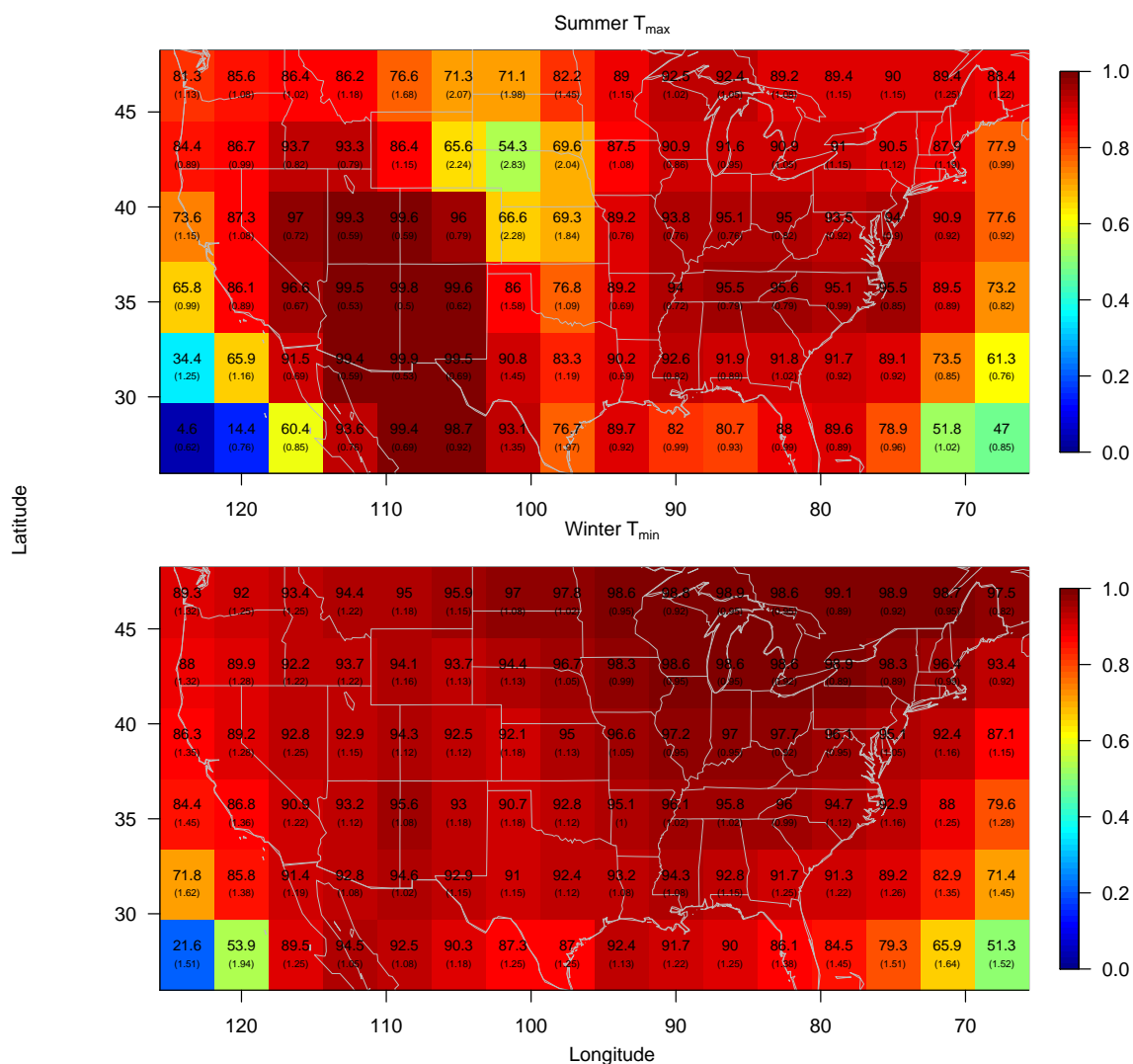


Figure A.3: The fraction of annual extremes that fall into the defined season (summer (JJA), winter (DJF)), shown both in color scale (0-1) and in numbers in large font (0-100). Numbers in parentheses are the interquartile range (IQR) of the distribution of the timing when annual extremes occur, in units of months.

To evaluate whether use of seasonal vs. annual means affects the analysis, we show changes in return levels (for a change in climate state from 289 to 700 ppm  $CO_2$ ) calculated using annual extremes. Results are almost identical to those obtained with seasonal means, except that the sharply rising “extreme extremes” in a few Midwest locations are less pronounced. (In these locations, use of seasonal means appears to produce artifacts.)

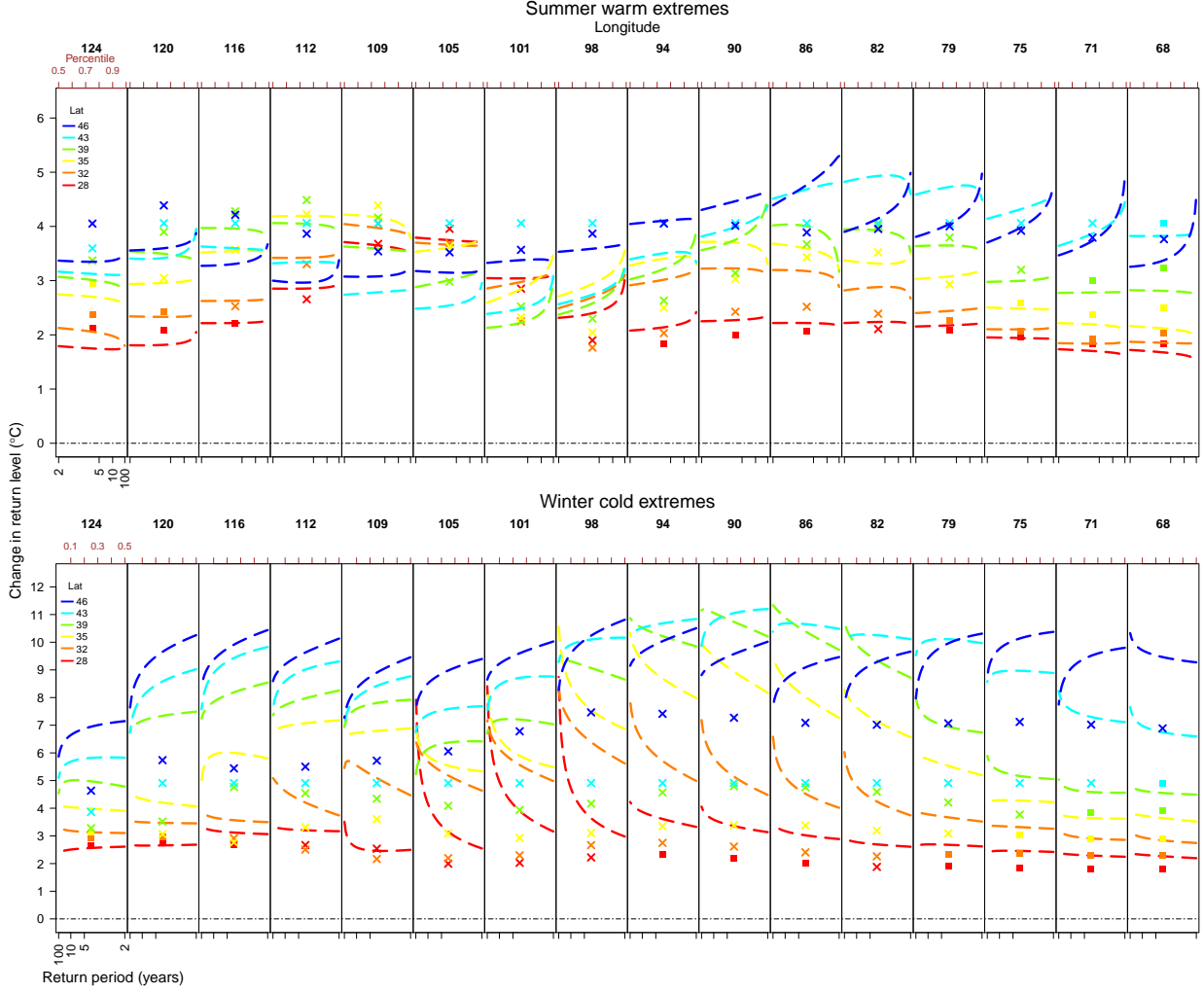


Figure A.4: Changes in return levels, as in Figs. 8 and 9 but for annual rather than seasonal extremes. We show only the “true” changes without estimated uncertainties. With the exception of a few locations, return level changes are almost identical regardless of whether annual or seasonal extremes are used.

### A.3 Extremal Types Theorem

In this appendix, we briefly describe the fundamental result in extreme value theory that justify the use of GEV model for block maxima. Let  $\{Y_i\}$  be a sequence of independent and identically distributed random variables with cumulative distribution function  $F$  and let  $M_n = \max\{Y_1, \dots, Y_n\}$ . When  $n \rightarrow \infty$ , the random variable  $M_n$  converge to a single point  $y_F = \sup\{y : F(y) < 1\}$ . In order to have a useful description of  $M_n$  when  $n$  is sufficiently large, normalization is needed, that is, we are seeking for limiting distribution for  $\frac{M_n - b_n}{a_n}$ . It turns out that if there exist constants  $a_n > 0$  and  $b_n$  and a non-degenerate distribution function  $G$  such that

$$\mathbb{P}\left(\frac{M_n - b_n}{a_n} \leq y\right) \xrightarrow{d} G(y)$$

then  $G$  must be of the same type (two random variables  $X$  and  $Y$  are of the same type if  $aX + b$  has the same distribution as  $Y$ ) as one of the three extreme value classes below:

$$\begin{aligned}
 \text{Gumbel: } G(x) &= \exp(-\exp(-x)) && -\infty < x < \infty; \\
 \text{Fréchet: } G(x) &= \begin{cases} 0 & x \leq 0, \\ \exp(-x^{-\alpha}) & x > 0, \end{cases} && \alpha > 0; \\
 \text{reversed Weibull: } G(x) &= \begin{cases} \exp(-(-x)^\alpha) & x < 0, \\ 1 & x \geq 0; \end{cases} && \alpha > 0,
 \end{aligned}$$

Conversely, any distribution function of the same type as one of these extreme value classes can appear as such a limit. The GEV distribution provides a convenient unifying representation of the aforementioned three types of distribution.

## A.4 GEV diagnostic

We use quantile-quantile plots to assess the appropriateness of fitted GEV distributions to model seasonal temperature extremes in the study region. For most of the locations, there is a good agreement between empirical quantiles and the fitted quantiles. This agreement holds across climate states and for both summer and winter extremes. (See Figs. A.5 and A.6.)

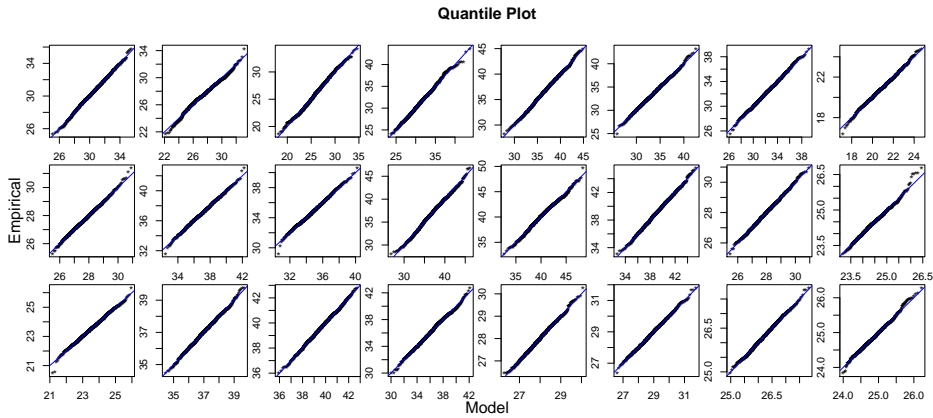


Figure A.5: The Q-Q plots for the fitted GEVs of warm extremes in pre-industrial climate. For clarity we display every other grid cell. (Model is run at T31 spatial resolution). These Q-Q plots show that GEV distributions provide reasonable approximations for annual summer maximum temperatures.

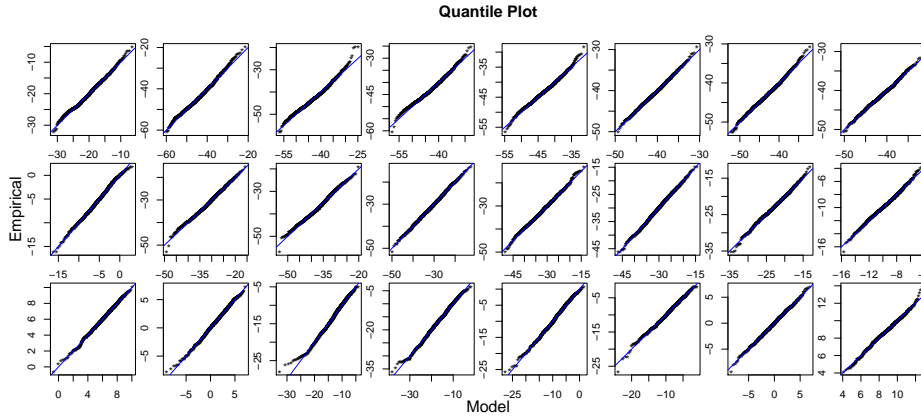


Figure A.6: As in Fig. A.5 but for winter cold extremes. Again, GEV distributions provide reasonable approximations for annual winter minimum temperatures.

## A.5 Model fitting procedures

The parameters of the extreme value distributions were fitted using maximum likelihood to the seasonal maxima/minima of each grid cell in the study region. The numerical optimization needed to find these estimates were performed by using the function `gev.fit` in the R package `ismev` (Stephenson and Heffernan, 2012). Return levels were obtained by plugging in the estimated GEV parameters into (3). Both simple nonparametric bootstrap (Efron, 1979) and moving block bootstrap (Künsch, 1989) were applied to seasonal extremes to assess the uncertainty of the changes in return levels. The block bootstrap allows us to take account of any dependence across years in seasonal minima or maxima; standard errors with different block sizes show little difference suggesting that extremes from one year to the next are nearly independent (see Fig. A.7).

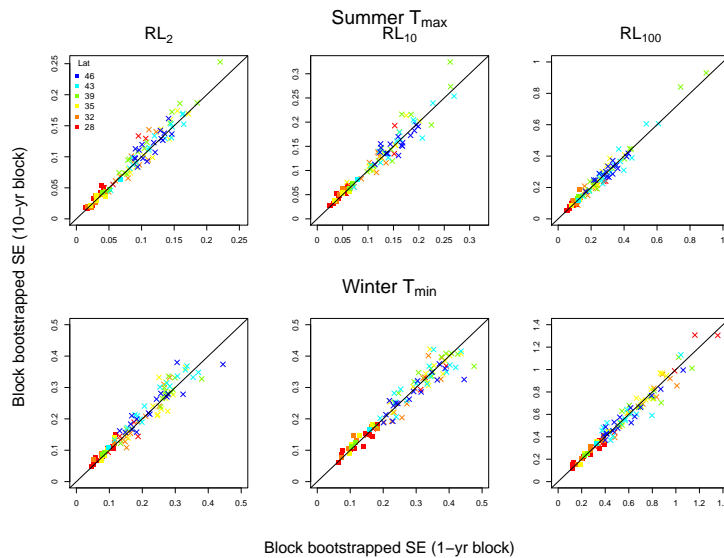


Figure A.7: The scatterplot of block bootstrapped standard errors by resampling years and decades, respectively. The plotted points fall on or near the line, meaning that the standard errors for block bootstrap with blocks of 1 year and blocks of 10 years are very similar.

## A.6 Relationships between changes in mean and changes in extremes

Here we explore the relationship of changes in extremes to changes in means, for both summer  $T_{\max}$  and winter  $T_{\min}$  (Fig. A.8). We find that the changes in the location parameter of warm extremes generally follow the mean changes during summer. Changes in the location parameter of cold extremes, however, are usually larger. For most inland locations, changes in winter cold extremes are amplified by more than 50% relative to changes in the average winter  $T_{\min}$ .

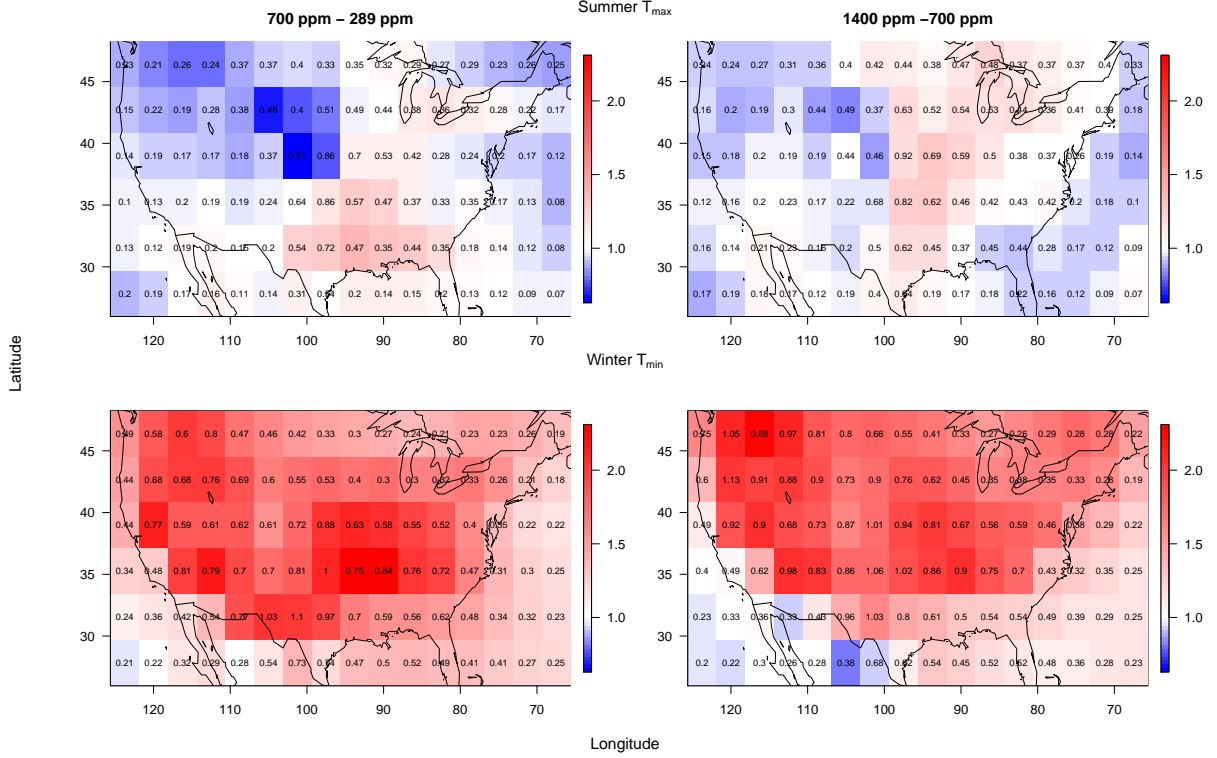


Figure A.8: The ratio of changes in estimated location parameters to changes in means (i.e.  $\Delta\mu_{\text{gev}}/\Delta\mu$ ) for summer  $T_{\max}$  (**upper**) and winter  $T_{\min}$  (**lower**). (**Left**) column shows change from pre-industrial to 700 ppm climate states; (**right**) column shows changes from 700-1400 ppm states. Red means the shift of the GEV distribution is larger than the shift of the overall distribution; blue means the inverse. Numbers are the bootstrapped standard errors ( $\times 10$ ) for  $\Delta\mu_{\text{gev}}/\Delta\mu$ . Those ratios are generally near 1 for summer  $T_{\max}$  and substantially greater than 1 for winter  $T_{\min}$  everywhere in the continuous United States.

## A.7 Changes in return levels: 1400 ppm versus 700 ppm

In this appendix we present results of changes in extremes of 1400 ppm versus 700 ppm. The spatial pattern of changes in return levels for summer warm extremes is similar to that of 700 ppm versus 289 ppm in which the location parameter changes play a dominant role in most pixels. Exceptions include a small part of the central Midwest corn belt region, which show rapid increases in return levels with return periods (see Fig. A.9, upper panel).

The decreasing downward pattern toward the lower tail of the changes in winter cold extremes for those high latitude pixels is less pronounced than that of 700 ppm versus 289 ppm mainly due the decreases in scale parameter (see Fig. A.9, lower panel).



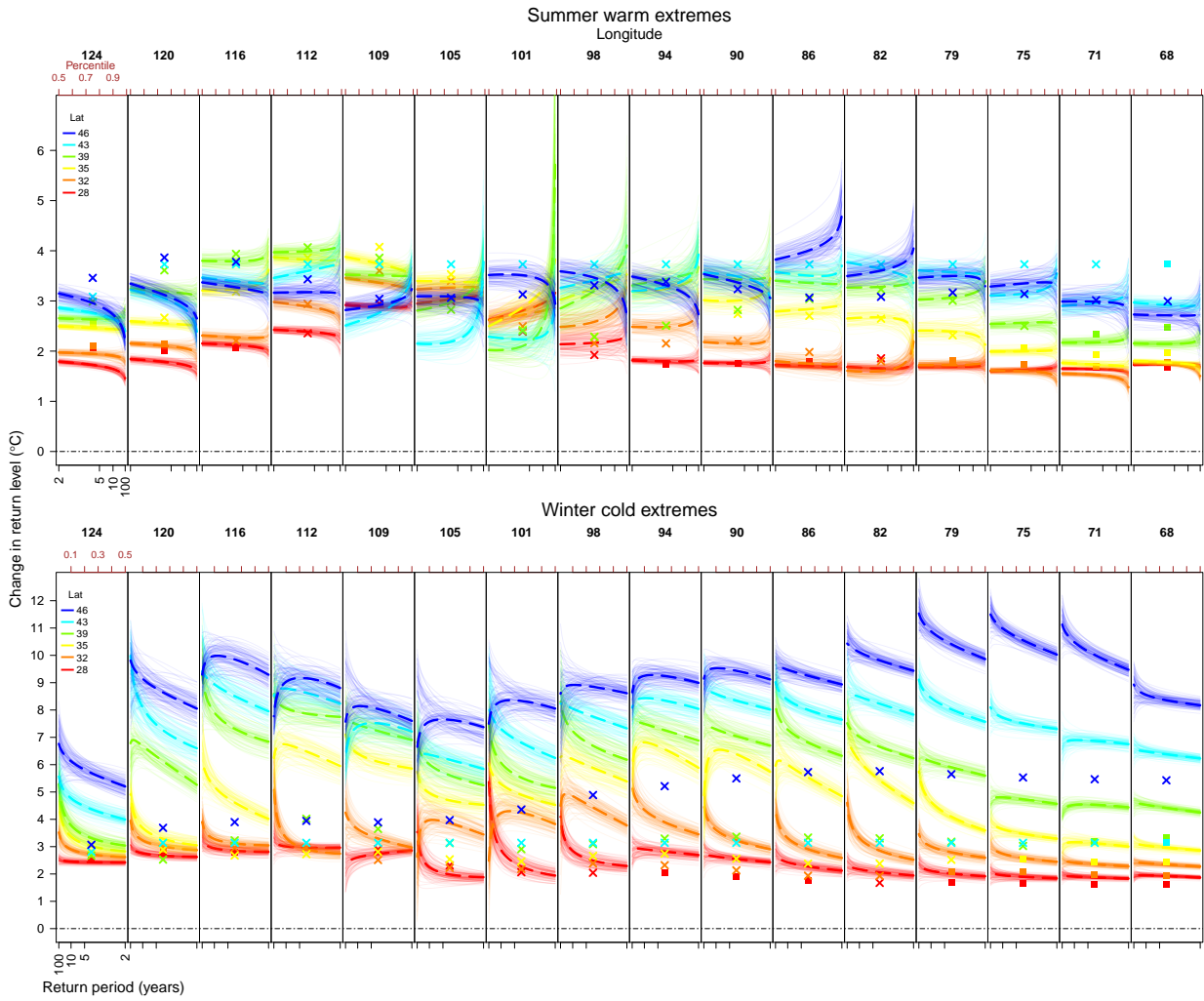


Figure A.9: Changes in return levels, as in Fig. 8 and 9 but here for changes from 700 ppm to 1400 ppm CO<sub>2</sub> climate states, rather than from pre-industrial to 700 ppm. Upper panel shows summer  $T_{\max}$  and lower panel shows winter  $T_{\min}$ . Summer changes are similar to those of Figure 8, confirming that changes in return levels for warm extremes are approximately linear with changes in climate means.